INTERIM REPORT

Quantification of Hydrodynamic Forcing and Burial, Exposure and Mobility of Munitions on the Beach Face

SERDP Project MR-2503

MARCH 2017

Jack A. Puleo
Brittany Bruder
Demetra Cristaudo
University of Delaware,
Center for Applied Coastal Research

SERDP
DOD ▪ EPA ▪ DOE

Page Intentionally Left Blank

Page Intentionally Left Blank

REPORT DOCUMENTATION PAGE

Form Approved
OMB No. 0704-0188

1. REPORT DATE *(DD-MM-YYYY)*	**2. REPORT TYPE**	**3. DATES COVERED** *(From - To)*
03-31-2017	SERDP Interim Report	9/14/2015 - 9/13/2019

4. TITLE AND SUBTITLE
Quantification of Hydrodynamic Forcing and Burial, Exposure, and Mobility of Munitions on the Beach Face

5a. CONTRACT NUMBER 15-C-0007

5b. GRANT NUMBER

5c. PROGRAM ELEMENT NUMBER

6. AUTHOR(S)

Puleo, Jack A.
Bruder, Brittany
Cristaudo, Demetra

5d. PROJECT NUMBER MR-2503

5e. TASK NUMBER

5f. WORK UNIT NUMBER

7. PERFORMING ORGANIZATION NAME(S) AND ADDRESS(ES)

University of Delaware
259 Academy Street
Newark, DE 19716

8. PERFORMING ORGANIZATION REPORT NUMBER

MR-2503

9. SPONSORING / MONITORING AGENCY NAME(S) AND ADDRESS(ES)
Strategic Environmental Research and Development Program
4800 Mark Center Drive, Suite 17D03
Alexandra, VA 20003

10. SPONSOR/MONITOR'S ACRONYM(S)

SERDP

11. SPONSOR/MONITOR'S REPORT NUMBER(S)
MR-2503

12. DISTRIBUTION / AVAILABILITY STATEMENT

DISTRIBUTION A. Approved for public release: distribution unlimited.

13. SUPPLEMENTARY NOTES

14. ABSTRACT

The objective is to quantify the hydrodynamic processes (velocity, shear stress, turbulence, surge) and associated munitions mobility (burial, exposure, transport) on the beach face. The pilot study was performed in the Littoral Warfare Environment (LWE) at Aberdeen Test Center (ATC) to quantify munitions mobility orientation, migration and burial depths while simultaneously recording the hydrodynamic forcing conditions and bed response. The pilot study is the first of its kind to simultaneously measure both processes on the foreshore under large scale conditions.

15. SUBJECT TERMS
Munitions, Surrogate Munitions, Inert Munitions, In Situ Sensors, Munitions Sensors, Mobility, Burial, Migration, Swash Zone, Foreshore, Sediment Transport, Sheet Flow, Boundary Layer

16. SECURITY CLASSIFICATION OF:			**17. LIMITATION OF ABSTRACT**	**18. NUMBER OF PAGES**	**19a. NAME OF RESPONSIBLE PERSON**
a. REPORT	**b. ABSTRACT**	**c. THIS PAGE**			Jack Puleo
Unclassified	Unclassified	Unclassified	Unclassified	49	**19b. TELEPHONE NUMBER** *(include area code)* 302-831-2440

Standard Form 298 (Rev. 8-98)
Prescribed by ANSI Std. Z39.18

Page Intentionally Left Blank

Table of Contents

List of Tables

List of Figures

List of Acronyms

ADPV	-	Acoustic Doppler Profiling Velocimeter (Vectrino II)
ATC	-	Aberdeen Test Center
AVT	-	Allied Vision Technology
CCP	-	Conductivity Concentration Profiler
EMCM	-	ElectroMagentic Current Meter
FOV	-	Field of View
GPS	-	Global Positioning System
IMU	-	Inertial Motion Unit
LWE	-	Littoral Warfare Environment
MR	-	Munitions Response
OBS	-	Optical Backscatter Sensor
PT	-	Pressure Transducer
SAB	-	Scientific Advisory Board
SUXOI	-	Swash Unexploded Ordnance Study I
SUXOII	-	Swash Unexploded Ordnance Study II
UXO	-	Unexploded Ordnance
WIMMX	-	Wallops Island Munitions Mobility Experiment

Keywords

Munitions
Surrogate Munitions
Inert Munitions
In Situ Sensors
Munitions Sensors
Mobility
Burial
Migration
Swash Zone
Foreshore
Sediment Transport
Sheet Flow
Boundary Layer

Acknowledgements

We would like to thank government employees Gene Fabian and Seth Lyter and contractors Carl Johnson, Carl Cramer, John Wertsch and Rick Fling for their assistance with SUXOI and SUXOII conducted at the Aberdeen Test Center Littoral Warfare Environment. Jonathan Harp of CHPT Manufacturing assisted in the design and was responsible for the fabrication of the surrogate munitions. Numerous researchers assisted during the studies: Ramy Marmoush, Peter Tereszkiewicz, Jose Carlos Pintado-Patino, Ryan Mieras, Douglas Krafft, Patricia Chardon-Maldonado, Matthew Doelp, Yeulwoo Kim, Michaela Maguire, David Polakoff, Stephen Napoli, Emily Robison, Nancy Zhou, Soupy Dalyander and Tim Nelson.

1. Objective

Our objective is to quantify the hydrodynamic processes (velocity, shear stress, surge) and associated munitions mobility (burial, exposure, transport) on the beach face. We performed a two studies in the Littoral Warfare Environment (LWE) at Aberdeen Test Center (ATC) to quantify munitions mobility orientation, migration and burial depths while simultaneously recording the hydrodynamic forcing conditions and bed response. These studies are the first to our knowledge to simultaneously measure these processes on the foreshore under large-scale conditions.

Our proposal is in direct response to the 2015 Statement of Need for the Munitions Response (MR) Program Area (MRSON-15-01), that calls for studies related to (1) assessing the environment for which munitions are found, and (2) environmental conditions, especially sediment type and hydrodynamic conditions, that are used to predict munition mobility and burial. To our knowledge, all previous and current SERDP funding related to the nearshore is focused in regions that are continually submerged. The proposed study is unique in that it seeks to understand munition mobility and processes controlling mobility in the region of the nearshore that is intermittently submerged (Figure 1). Our first large-scale study, SUXOI was conducted June 23-30 2016. Our second large-scale study, SUXOII, was conducted November 29 to December 7, 2016. The first field trial (WIMMX) at Wallops Island in collaboration with NASA and NRL was conducted March 6-24, 2017. The field trial will not be discussed further; with this report focusing on the LWE large-scale laboratory experiments.

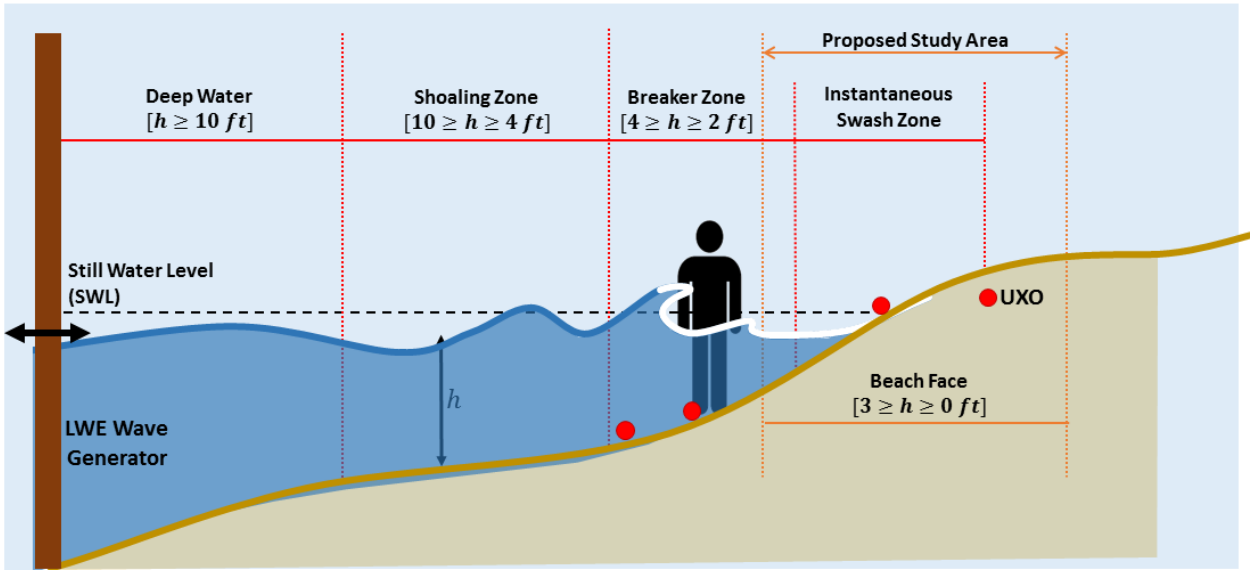

Figure 1. Schematic showing the nearshore region. The studies conducted under this proposal deployed surrogates and inerts in regions identified by the red dots.

We hypothesize that boundary layer conditions, specifically those in the sheet flow layer and the surge force govern munitions mobility on the beach face. Munition characteristics such as size,

shape and density must also play a role in mobility and several surrogate munitions spanning the parameter space were designed and constructed (see previous interim report). Our research will assist stakeholders focused on site remediation and management in understanding munitions mobility as it nears and/or reaches the beach face. Our research seeks to answer questions such as:

1) Does a munition that is stranded on the beach face (from dune erosion, excavated in place or delivered via transport from seaward), scour in partially, bury, or become transported offshore?
2) Does a munition that nears the shoreline reach the beach face or remain offshore?
3) How are the answers to 1-2 governed by forcing conditions and munition characteristics?
4) Do surrogate and inert munitions behave similarly under the same forcing conditions?
5) Can a simple force balance be used to determine munitions mobility on beaches? What is the overall importance of the surge force in landward transport of munitions when on the beach face?

Our measurements will provide data in an understudied region and complement data collected farther seaward in the surf (Traykovski, MR-2319) and shoaling regions (Calantoni, MR-2320) and provide needed data for process-based (e.g. Vortex Lattice UXO Model; D'Spain, MR-201234) and probabilistic (e.g. Underwater Munitions Expert System; Rennie, MR-2227) models on munition mobility.

The project is at a Go/No-Go decision point for the final field deployment to occur during the summer/fall of 2018. The Go/No-Go criterion as mentioned in the project brief to the Scientific Advisory Board (SAB; October 21, 2014) and in the final proposal is based on adequate progress from the large-scale studies and data analysis in consultation with SERDP program managers. We previously reported on the approach to develop smart surrogate munitions for mobility studies (6 different types) and some preliminary data from the first LWE study. We will not report again on the surrogate development but instead focus on the data analysis from the two LWE studies. Quality control and analysis for the WIMMX study is ongoing.

2. Technical Approach

Our technical approach includes detailed, time-dependent field measurements of munitions mobility/burial and concurrent hydrodynamic and bathymetric conditions under a variety of forcing scenarios. Several technologies (overhead and side looking imagery, imagery from submerged cameras, global positioning systems [GPS] and inertial motion units) are used to quantify munitions mobility. Simultaneous measurements of the hydrodynamic forcing were obtained using current meters, velocity profilers and pressure transducers. Sediment transport conditions were quantified using an array of optical backscatter sensors and conductivity concentration profilers (the sediment concentration data are less of a priority at this stage of analysis). Instruments were mounted to rugged scaffolding frames pounded into the beach face. We believe there is a dearth of data related to the detailed forcing characteristics and corresponding munitions mobility on the beach face under a range of forcing conditions.

This section describes the main instrumentation used during the studies and the study layout.

2.1 Sensors

In situ instruments (Table 1) were mounted to or near a scaffold frame (Figures 2 and 3) or to field tripods (Figure 4) depending on the location on the beach profile. Sensors on the field frame consisted of a Nortek Vectrino acoustic Doppler profiling velocimeter (ADPV), an array of four Druck pressure sensors (PT) offset in the vertical by 0.02 m, two Valeport electromagnetic current meters (EMCM) offset in the vertical by 0.03 m, three Campbell Scientific optical backscatter sensors (OBS) offset in the vertical by 0.03 m, two conductivity concentration profilers (CCP) offset in the vertical by 0.015 m and a Wenglor laser distance meter or Banner acoustic distance meter. Two Nortek Vectors were attached to the field tripods (Figure 4). RBR pressure sensors were deployed offshore to measure water level fluctuations. All sensor sample rates were chosen based on logging capabilities and the expected variability in the signal. The sensor layout was similar but not identical for both LWE studies.

Table 1. Sensors used during SUXOI and SUXOII.

Sensor	**Number**	**Logging Rate (Hz)**	**What it does**
Vector	2	64	Measures the 3 velocity components (u,v,w) at a single elevation 15 cm below the transducer
Vectrino II (ADPV)	1	100	Measures the 3 velocity components (u,v,w) over a 3 cm profile at 1 mm increments with the first bin beginning 4 cm below the transducer
Electromagnetic Current Meter	2	16	Measures the horizontal velocity (u,v) at a single elevation above the bed.
Optical Backscatter Sensors	3	16	Measures the amount of light backscattered off particulate matter in the water column. The measuring region is located in a cone in front of the sensor.
Pressure Transducer Array	4	16	Consists of 4 pressure sensors that measure absolute pressure separated by 2 cm in the vertical. Sensors are attached to a piece of rebar and buried in place. A 5^{th} sensor will be placed in air to measure atmospheric pressure.
Laser	1	16	A downward looking **eye safe** laser that measures time of flight. Distances from the sensor will be used to determine local water depth and bed level when the sand bed is exposed.
Conductivity Concentration Profiler	4	8	Measures the sediment concentration profile in the sheet flow layer at 1 mm vertical increments over 3 cm. Sensors deployed in pairs, attached to rebar and buried in place.
RBR pressure sensors	2	2	Measures absolute pressure to determine wave height and period

Figure 2. Picture showing field frame for deploying sensors. Sensors from left to right are: OBS array, EMCM pair, ADPV, Laser/Banner, underwater camera.

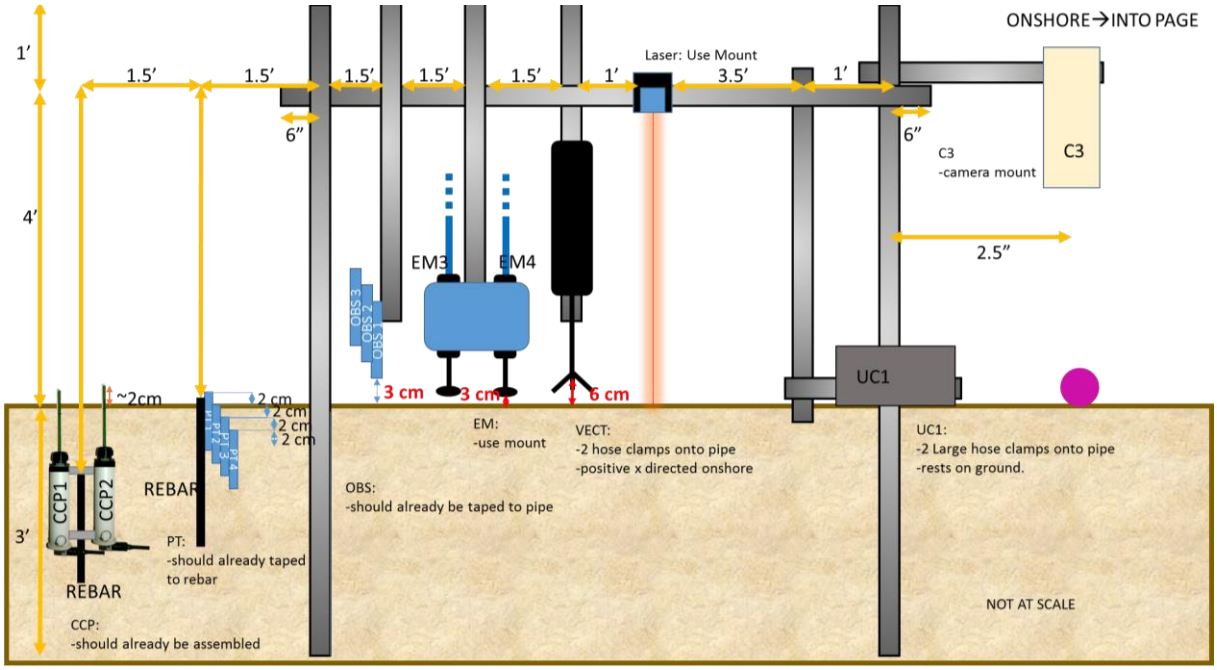

Figure 3. Schematic showing sensor layout on scaffold frame main array. The pink circle represents the location of a surrogate.

Figure 4. Picture showing tripod used to deploy Vector sensors offshore.

A variety of cameras were installed to capture images of the forcing conditions and the munitions mobility. Some cameras had the capability to be submerged while others were deployed away from the water. Table 2 shows the cameras used and their specifications. Deployment locations varied slightly between SUXOI and SUXOII.

Table 2. Cameras used during the pilot study at LWE.

Camera	**Location**	**Logging Rate (Hz)**	**What it does**
AVT Manta Camera	Tower 1	10	Collects video sequences of the experiment area (located on Tower 1)
AVT Prosilica GT1920 Camera	Tower 1	40 max	Collects video sequences of the experiment area but focused on the area of munition placement (located on Tower 1)
AVT Prosilica GC655 Camera	Frame	90 max	Collects video sequences of munition motion in the swash zone (downward-looking camera located on the frame)
AVT Prosilica GT1920 Camera	Flume wall	10	Collects video sequences of the surf zone area to capture float position (located near the trailer)
Dalsa Genie Camera	Frame	300 max	Collects video sequences of munition motion from the swash zone (side-looking camera located on the frame)
Splashcam	Tripod/Frame	30	Collects video sequences from the underwater offshore tripod

2.2 Littoral Warfare Environment Studies

The Swash UneXploded Ordnance mobility studies (SUXOI and SUXOII) were conducted from June 23-30, 2016 and November 29-December 7, 2016 in the LWE at ATC. The LWE is an outdoor wave flume that is 100 m long x 30 m wide and roughly 7 m deep (Figure 5). Waves are forced at the offshore boundary using 10 plunger wave paddles. Monochromatic or irregular waves can be forced for any particular duration. Waves used during the study were monochromatic or obtained from a Pierson-Moskowitz or JONSWAP spectrum. A total of 34 wave runs were completed in SUXOI and 25 runs in SUXOII with each run ranging from 2.5 to 10 minutes (Tables 3 and 4). Fewer runs for SUXOII occurred due to more rigorous surrogate position identification and the colder weather.

Figure 5. Picture showing the LWE facility looking offshore.

Table 3. Wave runs completed during the SUXOI study.

DAY	RUN#	Spectrum	Significant Wave height (m)	Peak Period (s)	Duration (min)	Start time	End time
June 27th	001	JONSWAP	0.52	3.282	5.0	6/27/2016 13:41	6/27/2016 13:46
	002	JONSWAP	0.64	3.637	5.0	6/27/2016 14:09	6/27/2016 14:14
	003	JONSWAP	0.91	4.798	5.0	6/27/2016 14:43	6/27/2016 14:48
	004				5.0	6/27/2016 15:19	6/27/2016 15:24
June 28th	005	JONSWAP	0.52	3.282	5.0	6/28/2016 8:59	6/28/2016 9:04
	006	JONSWAP	0.52	3.282	5.0	6/28/2016 9:36	6/28/2016 9:41
	007	JONSWAP	0.52	3.282	5.0	6/28/2016 10:03	6/28/2016 10:08
	008	JONSWAP	0.52	3.282	5.0	6/28/2016 10:26	6/28/2016 10:31
	009	PIERSON M	0.77	4.422	5.0	6/28/2016 10:48	6/28/2016 10:53
	010	JONSWAP	0.91	4.798	5.0	6/28/2016 12:38	6/28/2016 12:43
	011	JONSWAP	0.91	4.798	2.5	6/28/2016 13:08	6/28/2016 13:11
	012	JONSWAP	0.91	4.798	2.5	6/28/2016 13:24	6/28/2016 13:27
	013	JONSWAP	0.91	4.798	2.5	6/28/2016 13:40	6/28/2016 13:43
	014	PIERSON M	1.1	5.25	2.5	6/28/2016 13:55	6/28/2016 13:58
	015	PIERSON M	1.1	5.25	2.5	6/28/2016 14:14	6/28/2016 14:17
	016	PIERSON M	1.1	5.25	2.5	6/28/2016 14:39	6/28/2016 14:42
	017	PIERSON M	1.1	5.25	2.5	6/28/2016 15:00	6/28/2016 15:03
	018	PIERSON M	1.1	5.25	2.5	6/28/2016 15:33	6/28/2016 15:36
June 29th	019	JONSWAP	0.52	3.282	2.5	6/28/2016 15:33	6/28/2016 15:36
	020	JONSWAP	0.52	3.282	2.5	6/29/2016 9:17	6/29/2016 9:20
	021	PIERSON M	0.77	4.422	2.5	6/29/2016 9:34	6/29/2016 9:36
	022	PIERSON M	0.77	4.422	2.5	6/29/2016 9:54	6/29/2016 9:57
	023	JONSWAP	0.91	4.798	2.5	6/29/2016 10:13	6/29/2016 10:16
	024	JONSWAP	0.91	4.798	2.5	6/29/2016 10:34	6/29/2016 10:36
	025	PIERSON M	1.1	5.25	2.5	6/29/2016 10:56	6/29/2016 10:58
	026	PIERSON M	1.1	5.25	2.5	6/29/2016 11:22	6/29/2016 11:24
	027	MONOCR	0.30 (1ft)		10.0	6/29/2016 12:54	6/29/2016 13:05
	028	MONOCR	0.3		5.0	6/29/2016 13:26	6/29/2016 13:31
	029	JONSWAP	0.52	3.282	2.5	6/29/2016 13:57	6/29/2016 14:00
	030	JONSWAP	0.52	3.282	2.5	6/29/2016 14:12	6/29/2016 14:15
	031	JONSWAP	0.91	4.798	2.5	6/29/2016 14:31	6/29/2016 14:34
	032	JONSWAP	1.1	5.25	2.5	6/29/2016 14:51	6/29/2016 14:54
	033	JONSWAP	0.52	3.282	2.5	6/29/2016 15:12	6/29/2016 15:15
	034	JONSWAP	0.52	3.282	2.5	6/29/2016 15:31	6/29/2016 15:34

Table 4. Wave runs completed during the SUXOII study.

DAY	RUN#	Spectrum	Significant Wave Height (m)	Peak Period (s)	Duration (min)	Start Time	End Time
20161129	1	JONSWAP	0.9144	4.798	2.5	29-Nov-2016 13:34:37	29-Nov-2016 13:37:07
	2	JONSWAP	0.6427	3.637	2.5	29-Nov-2016 14:46:50	29-Nov-2016 14:49:20
20161130	3	JONSWAP	0.5242	3.282	10	30-Nov-2016 09:10:54	30-Nov-2016 09:20:54
	4	MONOCR	0.3	9	5	30-Nov-2016 10:23:28	30-Nov-2016 10:28:28
	5	JONSWAP	0.3311	2.609	2.5	30-Nov-2016 12:10:29	30-Nov-2016 12:12:59
	6	JONSWAP	0.6427	3.637	2.5	30-Nov-2016 12:56:22	30-Nov-2016 12:58:52
	7	JONSWAP	0.9144	4.798	2.5	30-Nov-2016 13:35:53	30-Nov-2016 13:38:23
20161201	8	MONOCR	0.3	9	5	01-Dec-2016 10:03:36	01-Dec-2016 10:08:36
	9	MONOCR	0.3	9	5	01-Dec-2016 10:58:00	01-Dec-2016 11:03:00
	10	JONSWAP	0.9144	4.798	2.5	01-Dec-2016 11:50:09	01-Dec-2016 11:52:39
	11	MONOCR	0.3	9	5	01-Dec-2016 13:11:03	01-Dec-2016 13:16:03
	12	PIERSON M.	1.1	5.25	2.5	01-Dec-2016 14:08:12	01-Dec-2016 14:10:42
20161202	13	MONOCR	0.3	9	5	02-Dec-2016 08:52:30	02-Dec-2016 08:57:30
	14	MONOCR	0.3	9	5	02-Dec-2016 10:06:01	02-Dec-2016 10:11:01
	15	PIERSON M.	0.777	4.422	2.5	02-Dec-2016 11:52:57	02-Dec-2016 11:55:27
	16	JONSWAP	0.9144	4.798	2.5	02-Dec-2016 12:51:37	02-Dec-2016 12:54:07
20161205	17	MONOCR	0.3	9	2.5	05-Dec-2016 09:41:22	05-Dec-2016 09:43:52
	18	MONOCR	0.3	9	5	05-Dec-2016 10:26:17	05-Dec-2016 10:31:17
	19	MONOCR	0.2	9	5	05-Dec-2016 11:18:26	05-Dec-2016 11:23:26
	20	JONSWAP	0.5242	3.282	2.5	05-Dec-2016 12:53:20	05-Dec-2016 12:55:50
	21	JONSWAP	0.9144	4.798	2.5	05-Dec-2016 13:49:32	05-Dec-2016 13:52:02
	22	MONOCR	0.6	7	2.5	05-Dec-2016 14:42:59	05-Dec-2016 14:45:29
20161206	23	MONOCR	0.3	9	5	06-Dec-2016 09:08:40	06-Dec-2016 09:13:40
	24	MONOCR	0.5	9	2.5	06-Dec-2016 10:22:45	06-Dec-2016 10:25:15
	25	MONOCR	0.3	9	2.5	06-Dec-2016 11:27:02	06-Dec-2016 11:29:32

The beach profile was shaped by heavy machinery when the facility was drained and prior to the initial run. The beach was made steeper for SUXOII than for SUXOI. Beach profiles were sampled using a real time kinematic GPS system (Figure 6) antenna mounted to a push dolly for SUXOI. The dolly was also used in SUXOII but additional offshore data were obtained from a boat using a second GPS system coupled with a sonar (Figure 7). The coupled system allowed the profile to be sampled almost to the wave paddles rather than solely where a researcher could wade. The profile was re-sampled every few wave runs in SUXOI and after every wave run in SUXOII to quantify the bathymetric change (Figure 8). The beach profiles changed throughout the study, forming an offshore sandbar and changing steepness. However, wave conditions during SUXOII were alternated in an effort to minimize drastic changes in beach shape.

Every sensor, pipe, tripod, tower etc. was also surveyed with the GPS system so spatial information was known. Data were then rotated into a local coordinate system that is roughly parallel with the flume wall.

Figure 6. Picture showing researchers surveying with the GPS push dolly.

Figure 7. Picture showing vessel used for offshore surveys. The GPS antenna can be seen to the lower right (covered by a plastic bag due to rainy conditions). The sonar is located directly below the GPS.

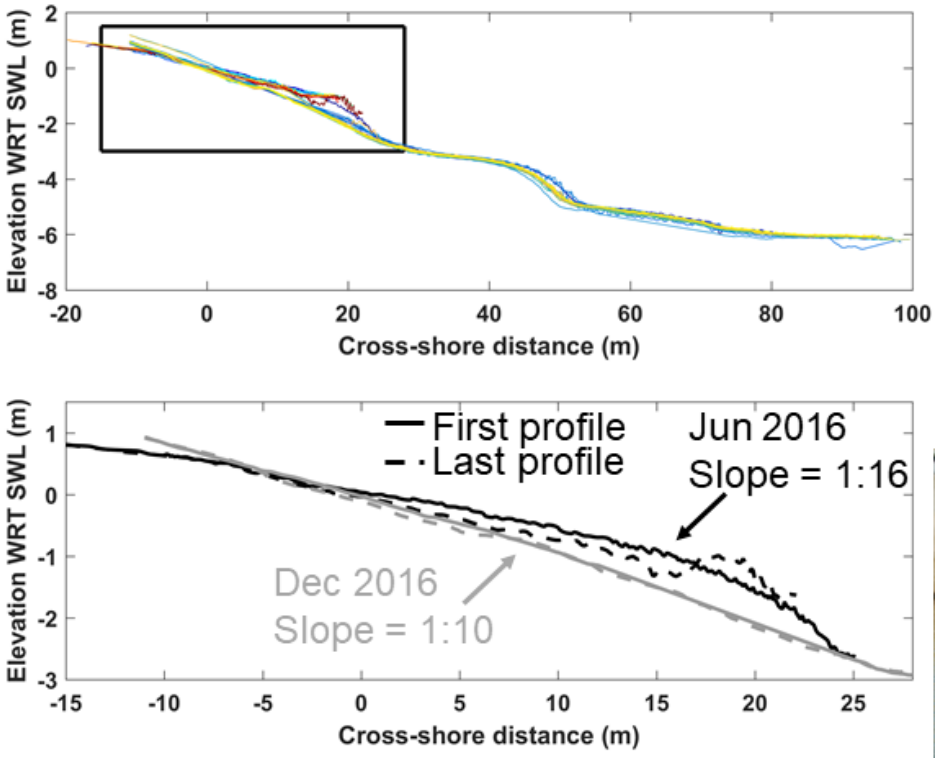

Figure 8. Bathymetry during the SUXOI and SUXOII studies. Colors in upper panel indicate different profiles. The lower panel shows the foreshore region and the different slopes. The slope for SUXOII was steepened to 1:10 rather than 1:16 as was used during SUXOI. The solid vs. dashed lines indicate the first and last profiles recorded during the respective studies.

Cameras were deployed from the various locations as mentioned earlier. The schematic of camera placement including rough fields of view (FOV) are shown in Figure (9). Targets were placed within the FOV enabling geo-rectification of imagery to the local coordinate system.

Figure 9. Schematic showing approximate fields of view during SUXOI. Similar fields of view were used during SUXOII.

All sensors and cameras were cabled back to a command trailer for power and communication (Figure 10). The command trailer contained many computers that controlled individual sensors through manufacture software, through MATLAB code written by the researchers or on a National Instruments data logger. Data were sampled only during the individual wave runs and according to the sample rates identified earlier. Computers were time synchronized through a local network running a time protocol obtained the time from a Garmin antenna, and using Dimension4 and Tac32 software.

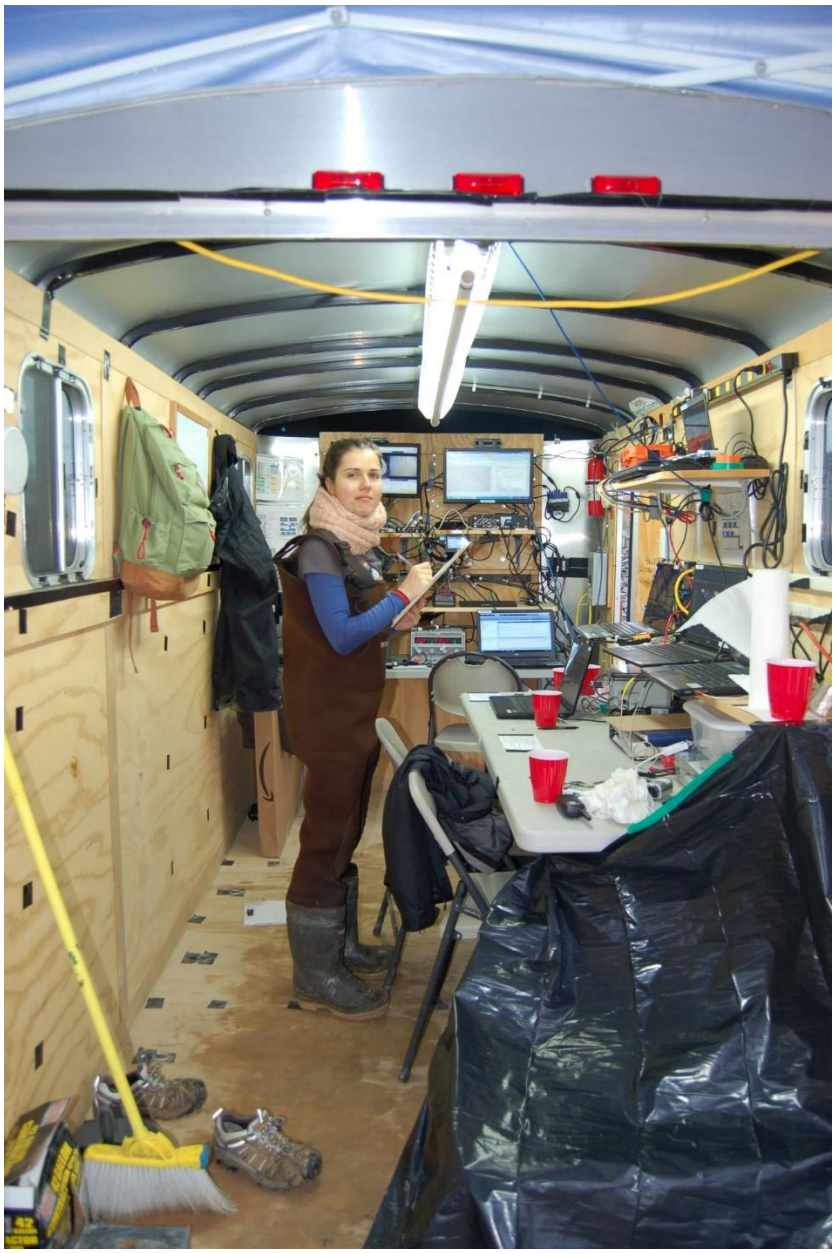

Figure 10. Command trailer and computer layout for the SUXO experiments.

Surrogate and inert munitions were placed in the surf zone (offshore and onshore of the breaker zone) and in the swash zone (Example shown in Figure 11). Surf zone surrogates/inerts were placed in an alongshore line and checked prior to the run for orientation and burial depth. Position was occasionally recorded because the surf zone surrogates/inerts did not move much. Swash zone surrogates/inerts were placed in clusters depending on the wave run and surveyed before and after the run to determine position, orientation and motion. Burial depth was also estimated. An alongshore fence offshore of the sensor frame was installed for SUXOII to trap surrogates before migrating into water deeper than researchers were permitted to go.

Figure 11. Schematic and pictures of surrogate and inert munitions placement in the surf and swash zones. Swash zone surrogate and inert munitions are located at or just landward of the still water shoreline. Surf zone surrogate and inert munitions are located (initially) landward and seaward of the typical breaking location. They can be seen through the water prior to the first wave run but subsequently cannot be seen due to opaque conditions. Small floats were attached to the items to help locate them but researchers often had to resort to a metal detector to find even proud munitions.

3. Results and Discussion

The Go/No-Go criterion as mentioned in the project brief to the Scientific Advisory Board (SAB; October 21, 2014) and in the final proposal is based on adequate progress from the laboratory

studies and data analysis in consultation with SERDP program managers. We have made great strides thus far n the project including: 1) complete design and construction of smart surrogate munitions that have correct geometry and weight characteristics; 2) undertaking two exhaustive large scale laboratory studies; and 3) ongoing analysis and paper writing based on the data from the studies. A short overview of the (ongoing) results from the SUXOI and SUXOII studies are described herein.

3.1 Data Quality Control and Analysis

Multiple terabytes of data were recorded during the two studies requiring extensive data quality control, cleaning and analysis procedures. There is a tradeoff between completely finishing all quality control before performing analysis or working in a hybrid fashion performing quality control while also analyzing the subsequent cleaned data sets. We have opted for the hybrid approach focusing on the measurements that we deem most critical. Table 5 shows the status of data quality control for the SUXOI and SUXOII studies respectively. The vast majority of data are cleaned and being used in sequence for the different analyses that are underway. At this stage, CCP data are a small component of the overall data set and not deemed critical for the ongoing analysis. The Velodyne and FARO lidars were used only during SUXOII and provide redundant data with the GPS at this stage.

Table 5. Status of data quality control and cleaning.

	SUXOI	SUXOII
GPS data	✓	✓
Vectrino	✓	✓
RBR PT	✓	✓
Data logger sensors	✓	✓
Vector	✓	✓
CCP		
FARO		
Velodyne		
Cameras	✓	✓
Munitions IMUs / data	✓	✓
LWE gauge	✓	✓

3.2 Example Forcing Conditions and Response – Observations

Tables 3 and 4 showed the variety of forcing conditions used during the LWE studies. Offshore waves shoal and break near the location where sensors were deployed and yield different local

hydrodynamics depending on the wave conditions. Some example conditions are shown in Figure 12 for monochromatic waves of 0.5 m offshore height and a 9 s wave period. The top panel shows the depth (blue) as recorded by the PT on the scaffold frame. The purple and green curves show depth recorded by PTs in 2 different Hydra Rocket surrogates. All signals are initially aligned. However, they diverge after the onset of a few waves. The rockets roll offshore into greater mean depth with the SUDRKT2 moving farther offshore than SUDRKT1. The phasing of wave arrival also shifts as expected with the rockets being located farther seaward. The corresponding velocity (2nd panel) measured at the sensor frame reaches nearly 2 m/s. Data gaps exist when the water retreats below the sensor or noise in the signal arises from initial inundation and bubbles. Panel 3 indicates the angular velocity measured by the IMU. Both rockets initially move offshore at roughly the same rate but then diverge. Some divergence is related to differences in rolling speed while sign differences are attributed to one rocket having spun 180 degrees relative to the other while still migrating offshore. Sensors inside the surrogates indicate short-lived acceleration spikes upon wave impact that can exceed 20 g (Panel 4). The larger spikes are observed from the Slamstick that records at a much higher frequency than the IMU.

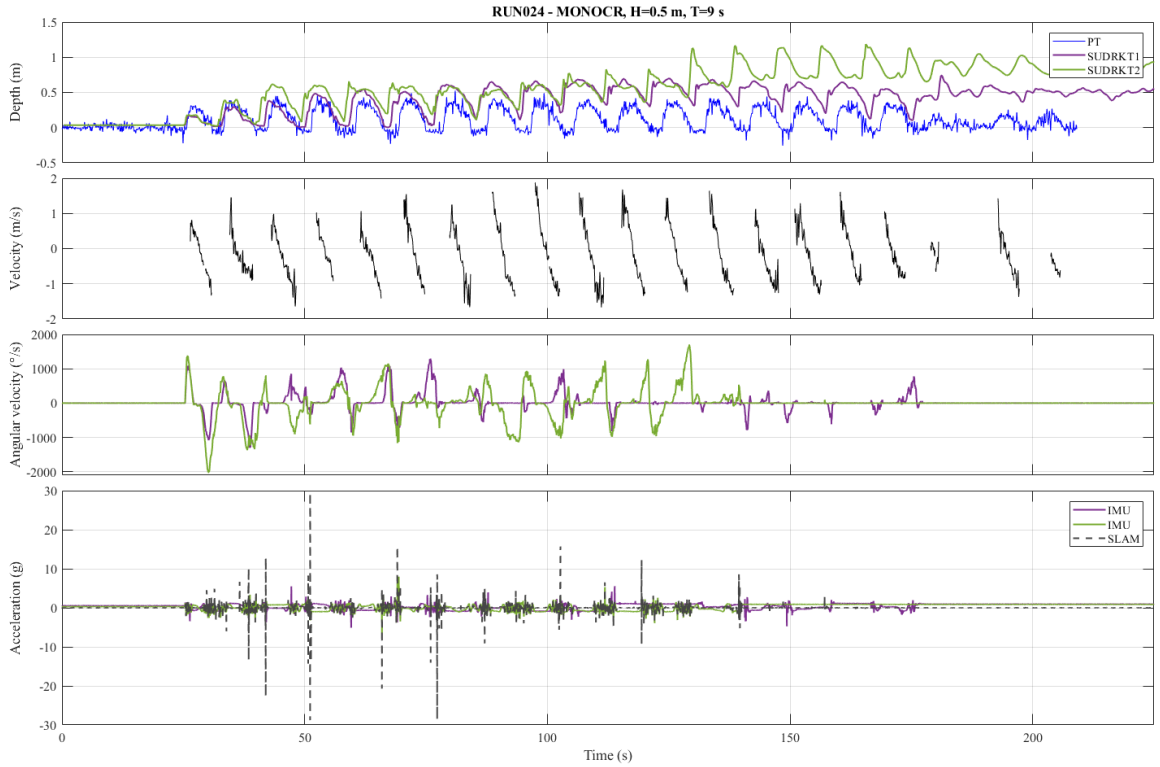

Figure 12. Example forcing conditions for RUN024 from SUXOII (monochromatic waves with a wave height of 0.5 m and period of 9 s). Top row: water depth at the scaffold frame (blue) and as measured by two the PTs within two different Hydra Rockets; 2nd row: Swash zone fluid velocity roughly 0.03 m above the bed; 3rd row: Angular velocity of the IMU located inside the Hydra Rockets; 4th row: Acceleration from the Slamstick and IMU located inside the Hydra Rockets.

Figure 13 shows a smaller excerpt of time from Figure 12 when the rockets were initially inundated. The frame PT signal is noisier than the rocket PT because it measures depth over a much wider range thus leading to larger variability at the smaller depths recorded here. Nevertheless, the signals align when the wave first arrives. The velocity (Panel 2) obtained in the swash zone is always discontinuous due to sensor elevation and noise upon immersion as already stated. However, velocities are needed for the duration of surrogate inundation. The velocity is largely governed by the downslope component of gravity and friction (black curve). Thus, a linear fit is applied to the velocity signal for each wave and extended back in time to the initial inundation point (pink curve). The third panel shows more clearly that the rockets rolled slightly onshore upon wave arrival and then rolled offshore during backwash. SUDRKT2 rolled offshore nearly twice as fast as SUDRKT1. Acceleration time series look quite noisy but this due to the fact the IMU is rotating through its main axis as the rocket rolls. Thus, the direction of gravity relative to the initial deployment orientation varies with rotation. What is clear is that the acceleration has an initial pulse upon inundation followed by a quiescent period during flow reversal. Accelerations then change signs rapidly as the rockets roll offshore.

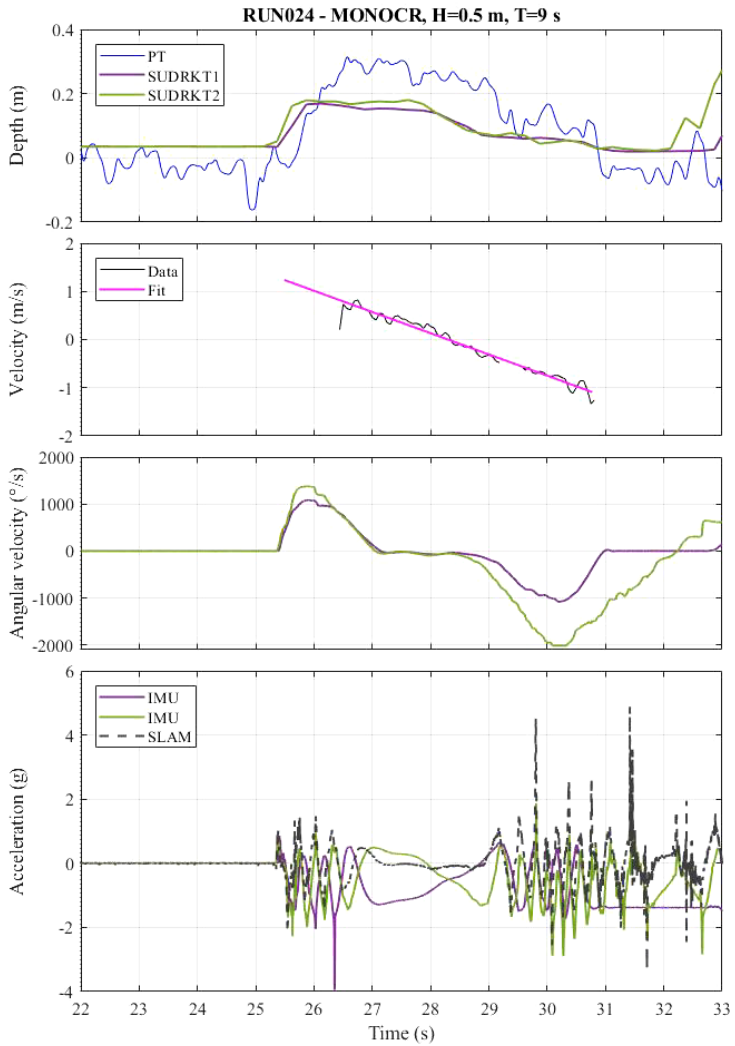

Figure 13. Short time series excerpt from Figure 12. Panel descriptions as per Figure 12.

Imagery (Figure 14) corresponding to the time series shown in Figures 12 and 13 helps to identify the processes occurring as well as variability (qualitatively in this example) between various surrogates and inerts. Four rockets and four 81 mm mortars were deployed just landward of the still water line for Run 024. Two of each type of munition are surrogates with the other two being inerts. The order of deployment is as follows from bottom top of Figure 14A (top to bottom of Figure 14A-1): surrogate rocket with an orientation of 0° (only the tip is visible in Figure 14A); inert rocket with an orientation of 0°; inert 81 mm mortar with an orientation of 90°; surrogate 81 mm mortar with an orientation of 90°; inert 81 mm mortar with an orientation of 90°; surrogate 81 mm mortar with an orientation of 90°; inert rocket with an orientation of 0°; and surrogate rocket with an orientation of 0°. Shortly after wave action, the rockets have rolled downslope or alongshore (Figure 14B and B-1). They mostly behave the same in that they tend to migrate offshore, but the travel distances and trajectories differ. The 81 mm mortars all initially behave the same with no motion. After more wave activity, the inert 81 mm mortars "wag" back and forth (presumably due to fins; *finless mortars will be tested in the upcoming field study*) and move offshore slightly. Surrogates and inerts do not appear to behave the same with surrogates remaining farther landward. This difference might be attributed to the lack of a nose cone in the inerts given the rest of the designs are consistent. Even the surrogate 81 mm mortars do not behave similarly with subsequent wave activity. One surrogate migrated several meters offshore while the 2nd surrogate remained mostly in place. In fact, the migrating surrogate has a final travel distance exceeding that of the inert 81 mm mortar.

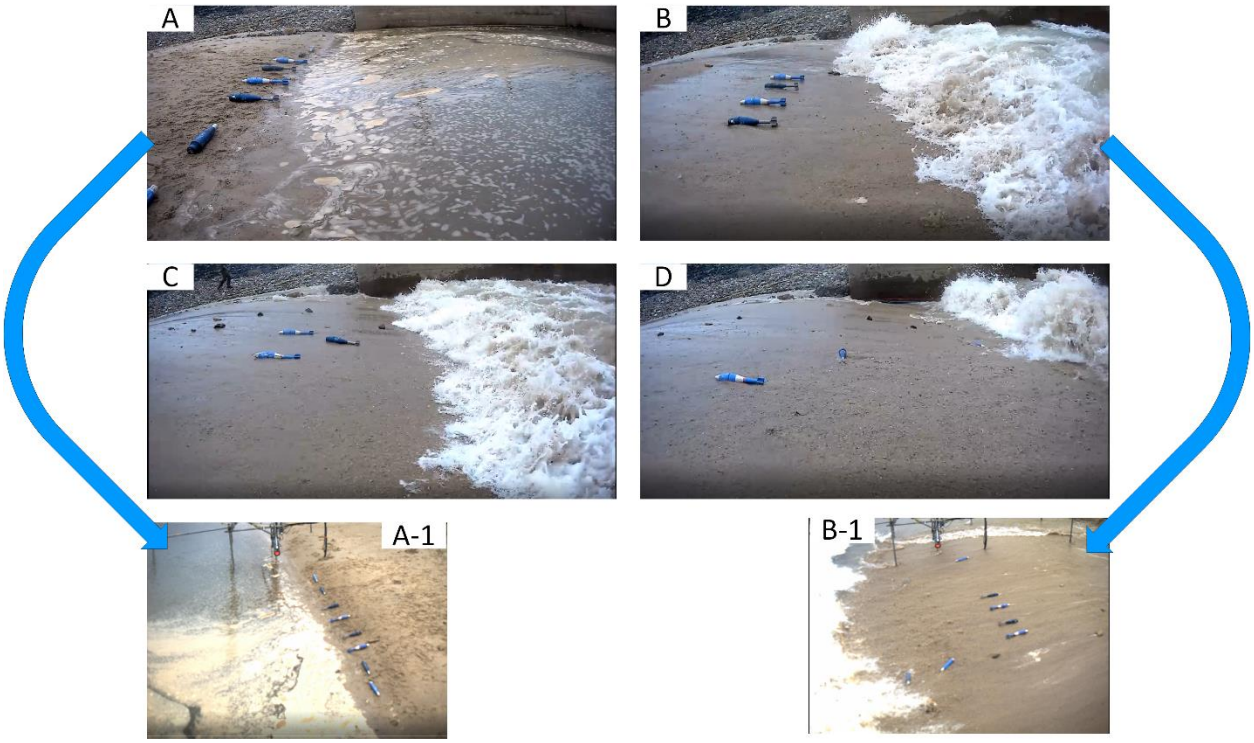

Figure 14. Imagery providing a qualitative view of the surrogate and inert motions for run 024 from SUXOII.

Figure 15 shows contrasting qualitative results of surrogate and inert motion from RUN020 (Jonswap spectrum with significant wave height of 0.52 m and period 3.28 s). Initial deployment (bottom to top of picture) contains a surrogate 155 mm Howitzer with an orientation of 0°, inert 155 mm with an orientation of 0°, two surrogate BLU 61 cluster bombs, inert 155 mm with an orientation of 90°, and a surrogate 155 mm Howitzer with an orientation of 90°. The surrogate and inert with an initial orientation of 0° roll downslope with the first few waves (Figure 15B). The other surrogates and inerts do not migrate and begin to bury in place. The surrogate and inert with an initial orientation of 0° have rolled farther downslope near the end of wave cessation and both maintain roughly the same orientation. The BLU 61 cluster bombs have scoured in roughly half way (B/D =0.5) and the other 155 mm Howitzers have scoured in only slightly.

Figure 15. Examples of surrogate and inert 155 mm Howitzer and BLU 61 cluster bomb motion under irregular wave forcing.

These qualitative observations are provided to indicate the variability in surrogate/inert motion as well as the variability even for the same type of object under the same forcing conditions. It is believed that even slight variations in local bathymetry or even offshore bathymetry altering

local wave shoaling or refraction must play a role in how the munitions on the beach face respond to wave action.

3.2 Example swash zone migration results obtained from inertial motion units and imagery

We presented in the previous report time series of surrogate and inert motion as obtained from GPS data and manual measurements. Here we focus on swash zone migration results obtained from GPS data and IMUs as well as that obtained from imagery.

3.3.1 IMU Results

IMU gyro data around the x-axis (longitudinal) are used to obtain the cumulative angle of rotation of the munition. These data are coupled with munition diameter to obtain a migration distance. Data from two different munitions from RUN025 are shown as an example of the capability of the simple technique. IMU-based position data are compared to manual identification in corresponding imagery following image rectification (Figures 16 and 17). The GPS identified initial and final locations are also identified (pink squares). The image identified and GPS identified locations are essentially the same as expected. The SUD811 (81 mm surrogate; Figure 16) start with an initial orientation of angle of 90° with the surrogate tip identified by the filled colored circle. Time elapsed is identified by the color bar as well as with numerals in the left panel. The surrogate rotates to roughly parallel to the waves and travels offshore (time up to 46.47 s). It then migrates onshore roughly 1 m before again migrating offshore approximately 2 m. The final GPS position roughly corresponds with the last position identified in imagery but it must be borne in mind that after the surrogate enters the opaque water in a region where backwash recession does not enable it to be seen, no position can be identified in the imagery. The IMU derived position roughly matches that of what is obtained from the imagery but exceeds the final GPS cross-shore position by approximately 0.5 m. One reason might be the assumption of solely cross-shore migration. However, the surrogate may be oriented oblique to the flow field and thus have an oblique (relative to cross-shore) migration path. This obliquity would overestimate the distance traveled in the cross-shore and underestimate the migration in the alongshore.

Figure 17 shows the same type of motion but for SUDRKT1 (surrogate Hydra Rocket). Note the variability in orientation and position as identified from the imagery. Again, image-based position cannot be ascertained after roughly 47 s due to the rocket no longer being visible. Thus, the difference between the GPS final position and that observed in the imagery are NOT expected to be the same. Here, the estimate of cross-shore position from the IMU has more error. The calculation suggests only roughly 0.5 m of offshore motion whereas the GPS data indicate roughly 3.5 m. Imagery corresponding to several of the instants where image-based position data were obtained are shown in Figure 18.

We are still working on the best algorithms to derive position from low-cost IMU data. Rapid movement over short time intervals make the estimate difficult as compared to data obtained farther offshore where the motion is slower and less frequent. There, simple filtering algorithms are more readily applied by forcing the acceleration or roll data to zero when it is “known” the object is not moving even though the actual time series has some noise about this zero value.

Applying the same concepts on the sloping beach are not as straightforward. Additionally, the use of the roll angle has complications if the object is not rolling directly offshore (oblique) and/or there is a component of sliding to the motion that will not be captured in the gyroscope data. Yet, we believe the double integral of acceleration for a rapidly rolling object is even more fraught with potential error. We are less confident in the present approach for alongshore motion as different surrogate behavior can more severely skew the estimated travel distance. The IMU GPS and imagery will aid in refining the position algorithm. Data such as in Figures 16 and 17 identify the timestamp when the approach IMU fails (i.e. at second 46 in Figure 17), providing an opportunity to more closely scrutinize the IMU data. The next step will involve more analysis on the angular velocity signal related to the other two axes of the munition to resolve alongshore migration. It will require deriving the orientation of the munition at each instant of time (based on the angular velocity of the longitudinal axis) that leads to the derivation of the longshore path due to the angular velocity of the other two axes.

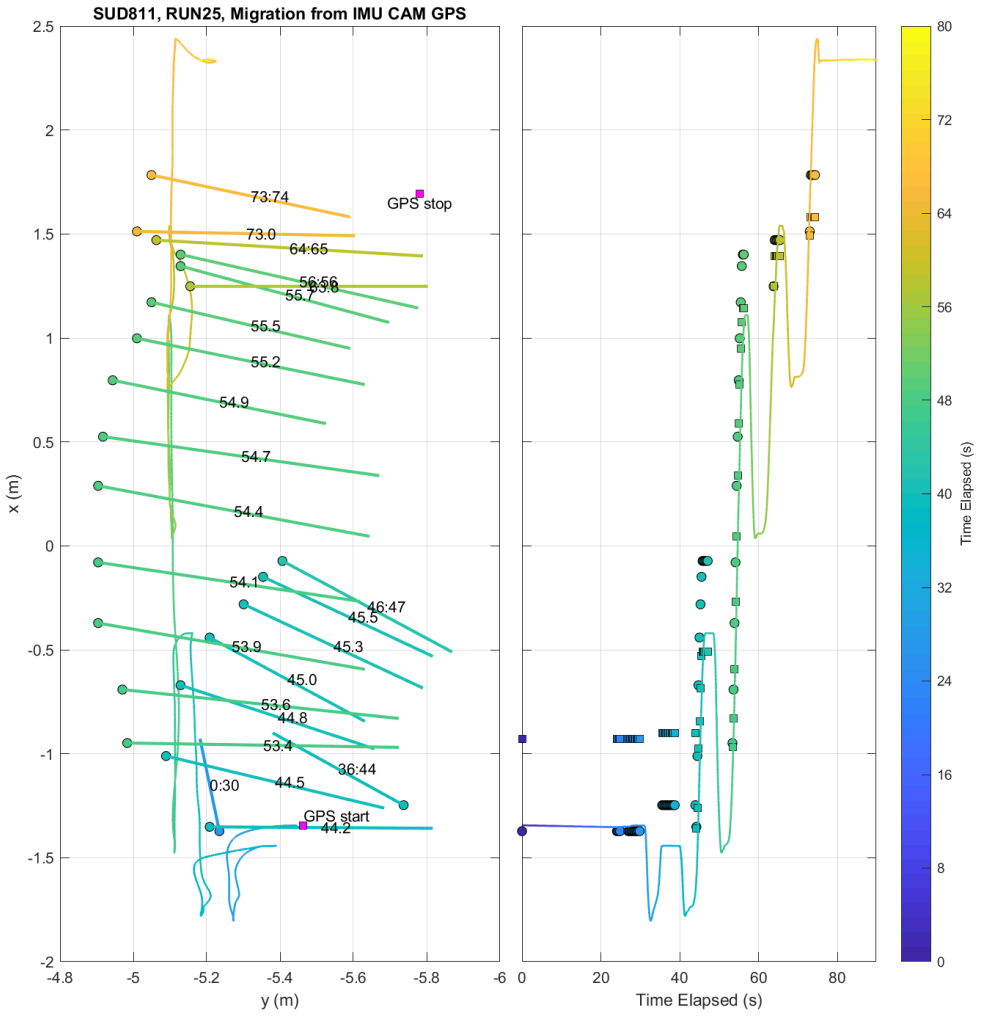

Figure 16. IMU (curve) and image-based position of the SUD811 (surrogate 81 mm mortar) for RUN025. The filled color circle represent the surrogate tip while the filled color squares indicate the surrogate base (squares in the right panel only). The color scale identifies the relative time in the run. GPS start and stop locations are identified by pink squares.

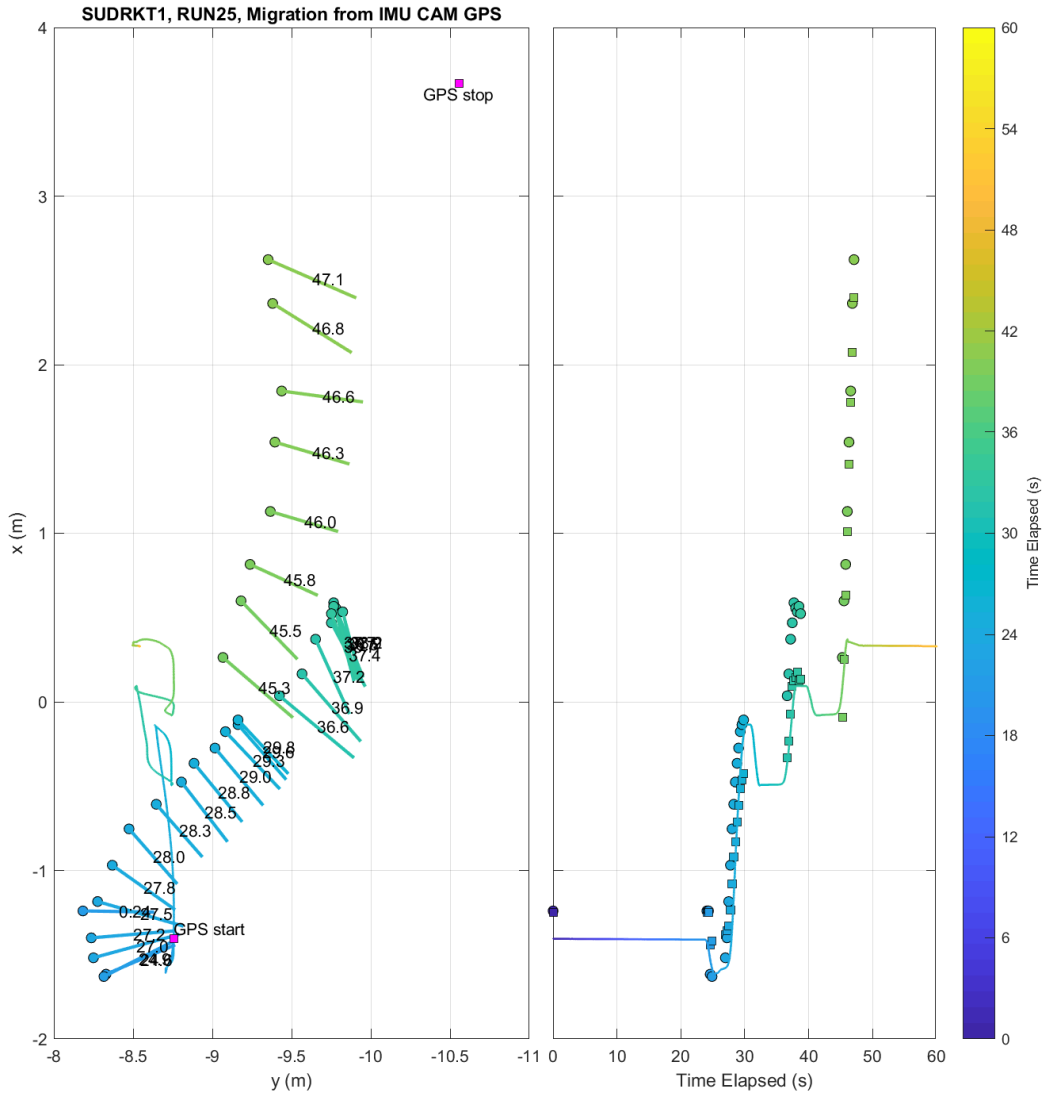

Figure 17. IMU (curve) and image-based position of the SUDRKT1 (surrogate Hydra Rocket) for RUN025. The filled color circle represent the surrogate tip. The color scale identifies the relative time in the run. GPS start and stop locations are identified by pink squares.

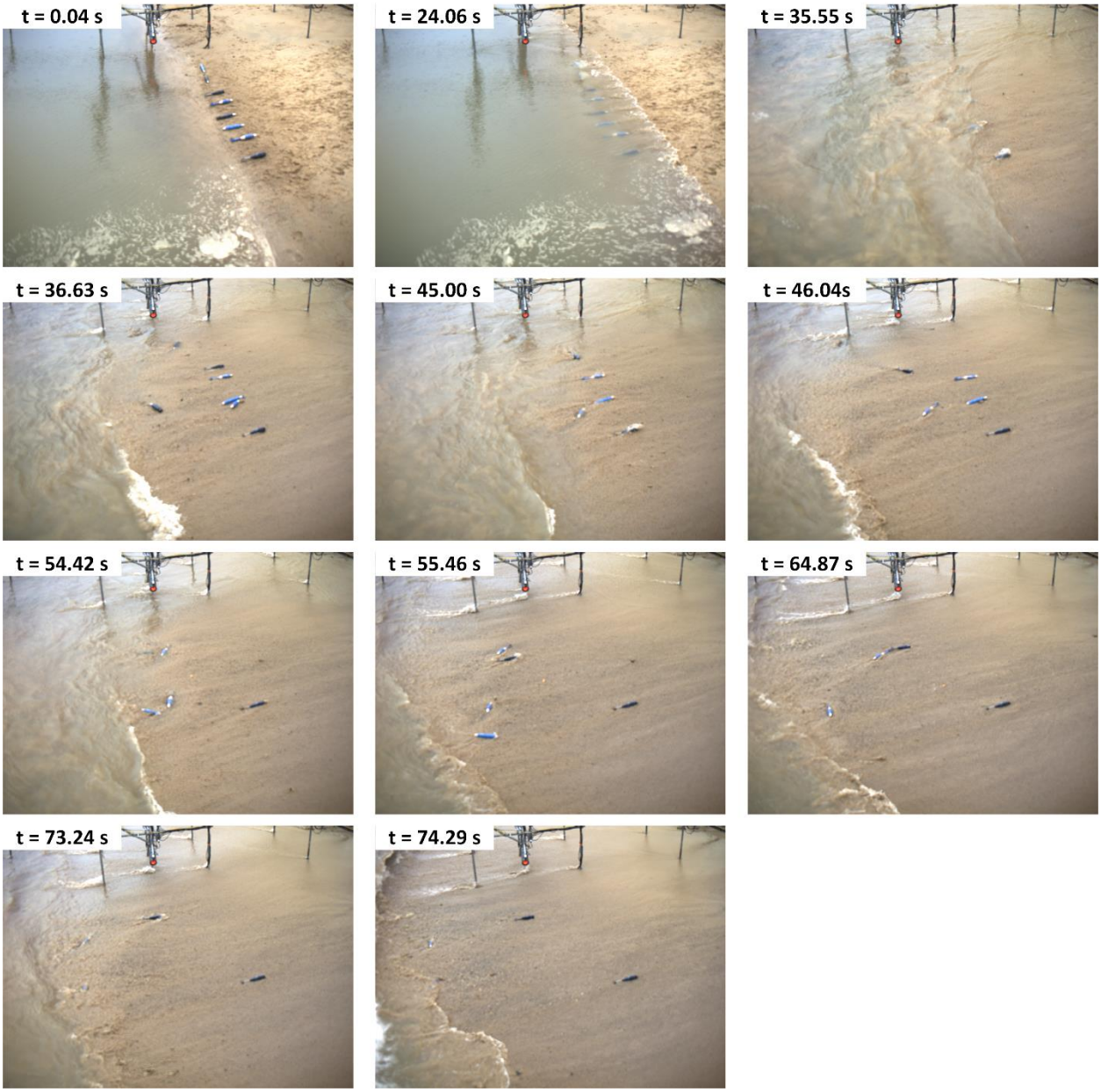

Figure 18. Image sequence from RUN025 showing some frames where position data were extracted.

3.3.2 Position Data Overlain on Timestack Imagery

Images were geo-referenced using the method of Holland et al. (1997) based on multiple targets surveyed into the local coordinate system. Figure 19 shows the oblique and geo-referenced image from RUN025. Note that the conversion from 2d image coordinates to 3D real world coordinates is underdetermined and thus one coordinate must be specified. The tide level is normally used for offshore imagery not showing the beach. Here we "warp" the image to the beach slope since the focus is mainly on swash processes. The intended consequence of this type

of rectification is that the munitions of interest are located ON the beach face such that identifying their position in the geo-referenced imagery provides an accurate estimate of cross-shore and alongshore position (See Figures 16 and 17).

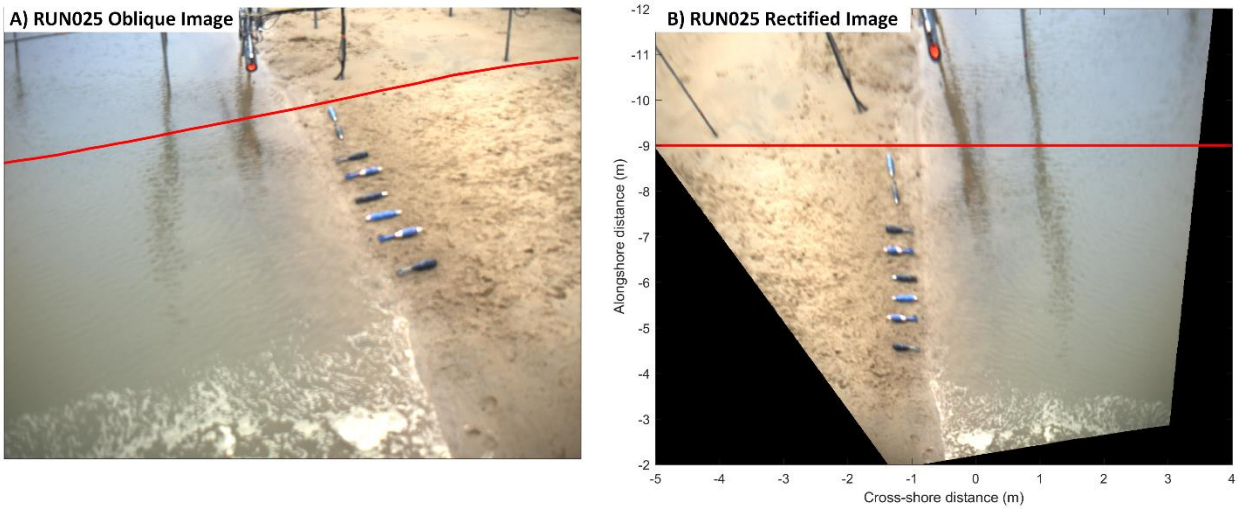

Figure 19. Oblique (A) and rectified imagery (B) for RUN025 both showing the pixel transect line (red) used to generate the timestack.

Munitions motion can be more clearly viewed in relation to forcing by developing a timestack image and overlying the position data. Timestacks are created by extracting a pixel intensity line from every geo-referenced image (the red line in Figure 19A and 19B) and placing into a matrix. All the surrogate and inert positions from the rockets and 81 mm mortars are shown on the timestack from this run (Figure 20). Surrogates and inerts are difficult to see in the turbulent uprush front but are visible during backwash. Their position, as identified by the symbols, tracks well with the backwash flows observed in the timestack. Some surrogates and inerts moved rapidly offshore while others had more intermittent motion (these variations in motion have been identified from previous figures). A major benefit to the timestack is the coordinate system being space-time such that the slope of any feature or curve fit through surrogate or inert positions quantifies the velocity. This means that the object and/or fluid velocity associated with munitions mobility can be estimated at the time-dependent position of the munition rather than relying solely on data from the fixed frame. We will be investigating use of these velocities in forthcoming analyses but for now use the current meter derived velocities for analyses presented here.

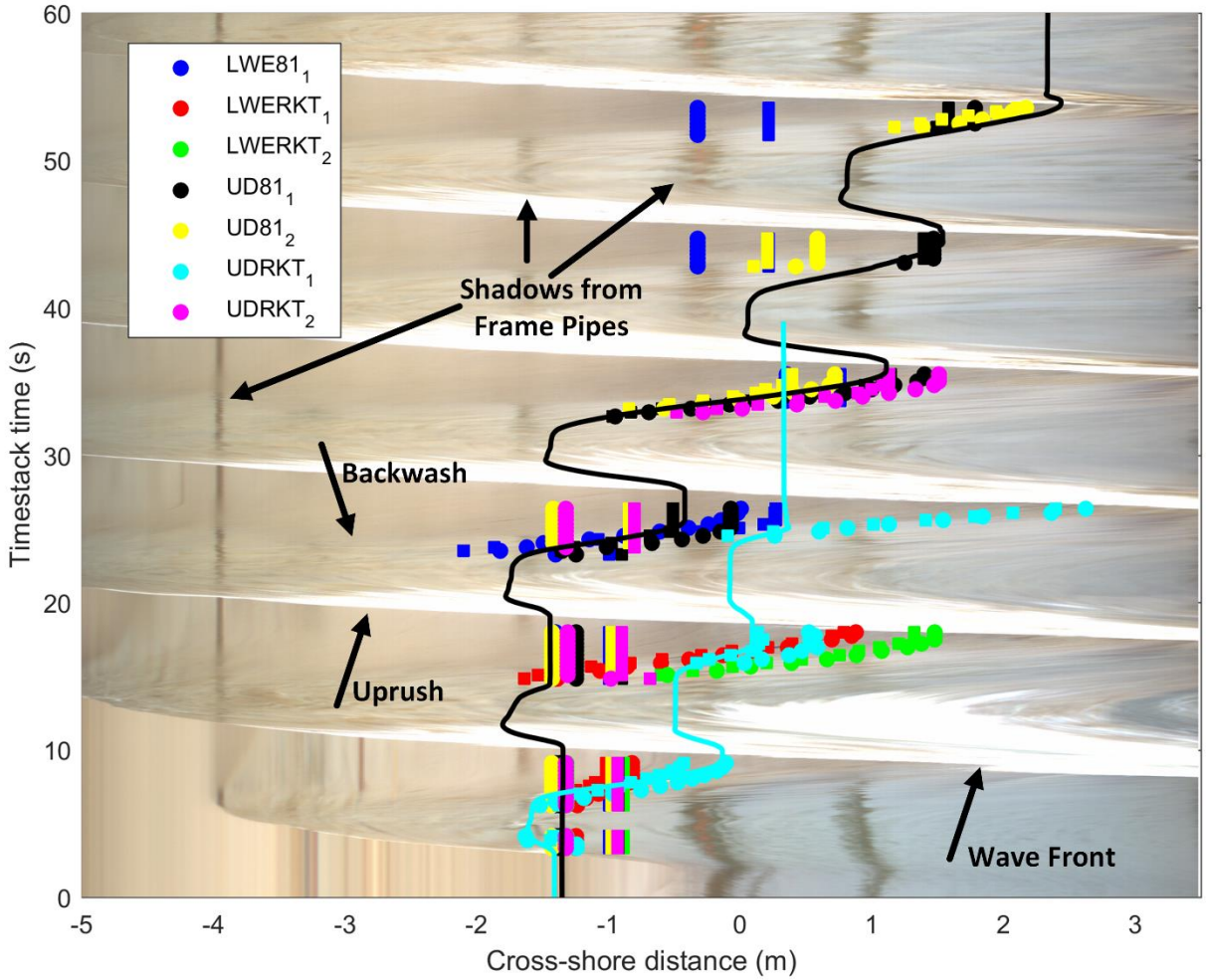

Figure 20. Image timestack from RUN025 with overlain positions of surrogate and inert munitions identified from georeferenced imagery (symbols: tips are filled circles, bases as filled squares) and from IMU estimates (curves).

3.4 Example migration and burial results compared to dimensionless parameters

Prior data suggest that common dimensionless fluid dynamic parameters may be able to explain some of the variance in observed munitions motion and mobility (Friedrichs et al., 2016; Rennie et al., 2017). The Shields number, θ, is a ratio between the stabilizing and destabilizing forces of a sand grain on the beach face. The Shields number is defined as

$$\theta = \frac{\tau}{\rho(s-1)gd_{50}}, \quad (1)$$

where τ is the bed shear stress, ρ is the fluid density, s is the ratio of sediment to fluid density, g is gravitational acceleration and d_{50} is the median sediment diameter. The shear stress can be parameterized numerous ways where here the simplest, a quadratic drag law, is employed as

$$\tau = \frac{1}{2}\rho f u^2, \tag{2}$$

where f is a friction factor and is on the order of 0.01 for sandy beaches (Puleo and Holland, 2001).

Another dimensionless parameter of interest is the Keulegan-Carpenter (KC) number that is the ratio between drag and inertia forces. The KC number is defined as

$$KC = \frac{uT}{D}, \tag{3}$$

where u is a characteristic flow speed, T is an orbital motion duration; here the swash duration, and D is the object diameter.

Migration of surrogate (Figure 21, squares) and inert munitions (Figure 21, circles) shows an obvious dependence on θ with little migration for θ below approximately 5. Note that the transition to sheet flow is thought to occur near $\theta = 1$. Surrogates and inerts show similar trends in general but the variability between just surrogates or just inerts for similar forcing conditions indicates a wide range of possible travel distances; something alluded to in the qualitative image analysis discussed before. Munitions are grouped here based on density rather than munition type as density is thought to be a key parameter in migration and burial. Objects migrate farthest offshore and onshore for the least dense surrogates. Offshore migration is greatest for the inert items and these inert items were 155 mm Howitzers that had roughly 10 kg less mass than the true munition or surrogate. Except for these “lighter” munitions, there was not a large dependence on beach slope with respect to migration as a function of Shields number. The lack of dependence is probably because both slopes are fairly steep and the difference between 1:10 and 1:16 is not enough to significantly alter surrogate or inert behavior.

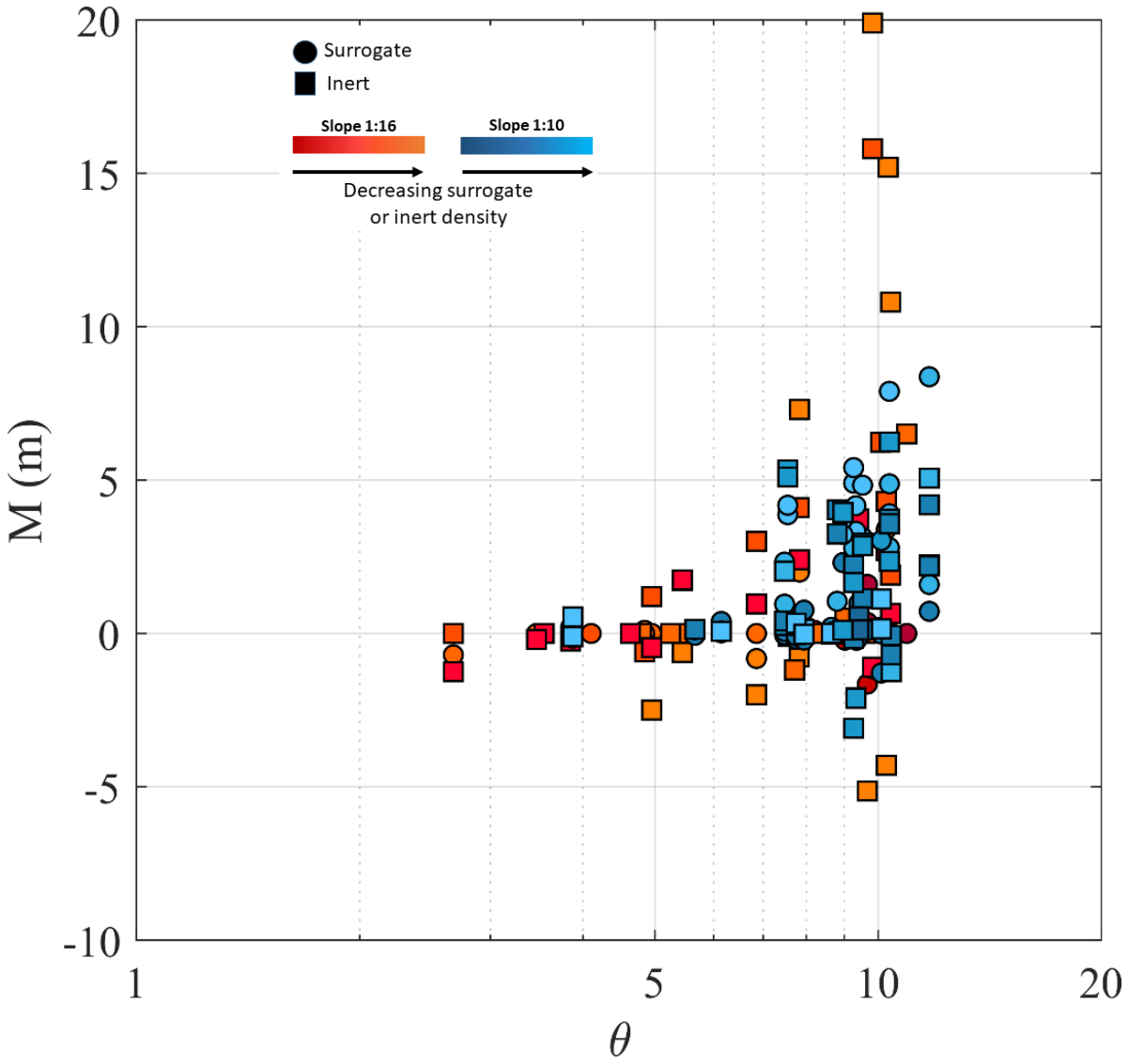

Figure 21. Cross-shore swash-zone surrogate and inert munitions migration as a function of object density, foreshore slope and Shields number. Density scale varies from roughly 3300 kg/m^3 to 8000 kg/m^3.

The relative burial depth, *B/D*, as the burial distance divided by the object diameter, does not show a strong dependence on θ (Figure 22). There is, however, some dependence as the more dense objects scour in at higher Shields number (shearing stresses). The objects with *B/D* greater than 1 were the 20 mm and occasionally 40 mm rounds. We note, though that the error in measuring burial depth is estimated to be roughly 0.01 which is a large fraction of the diameter of these small objects.

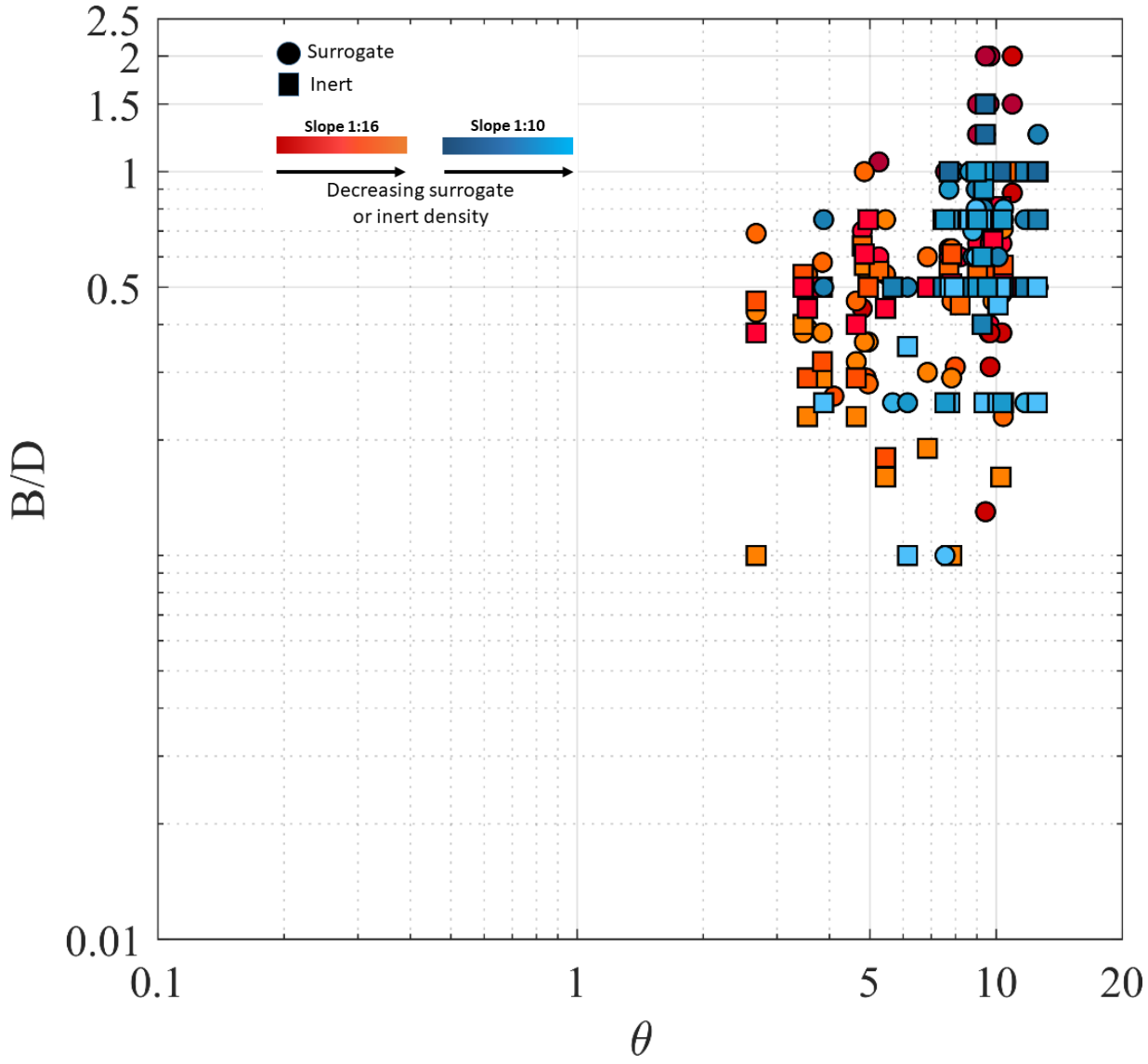

Figure 22. Relative burial depth of swash-zone surrogate and inert munitions as a function of object density, foreshore slope and Shields number. Density scale varies from roughly 3300 kg/m^3 to 8000 kg/m^3.

Surrogate and inert munitions do not show a consistent trend in migration in relation to the KC number (Figure 23). There is some increase in migration with increasing KC for the steeper slope but not for the more dense objects. The dense objects on the shallower slope do not migrate even under KC exceeding 100. The inert objects that migrate the farthest under moderate KC number were the "lighter" 155 mm inerts (used in the SUXOI study) that are essentially large lightweight cylinders. Correctly scaled inerts used in the SUXOII study behaved more similar to the fabricated surrogates.

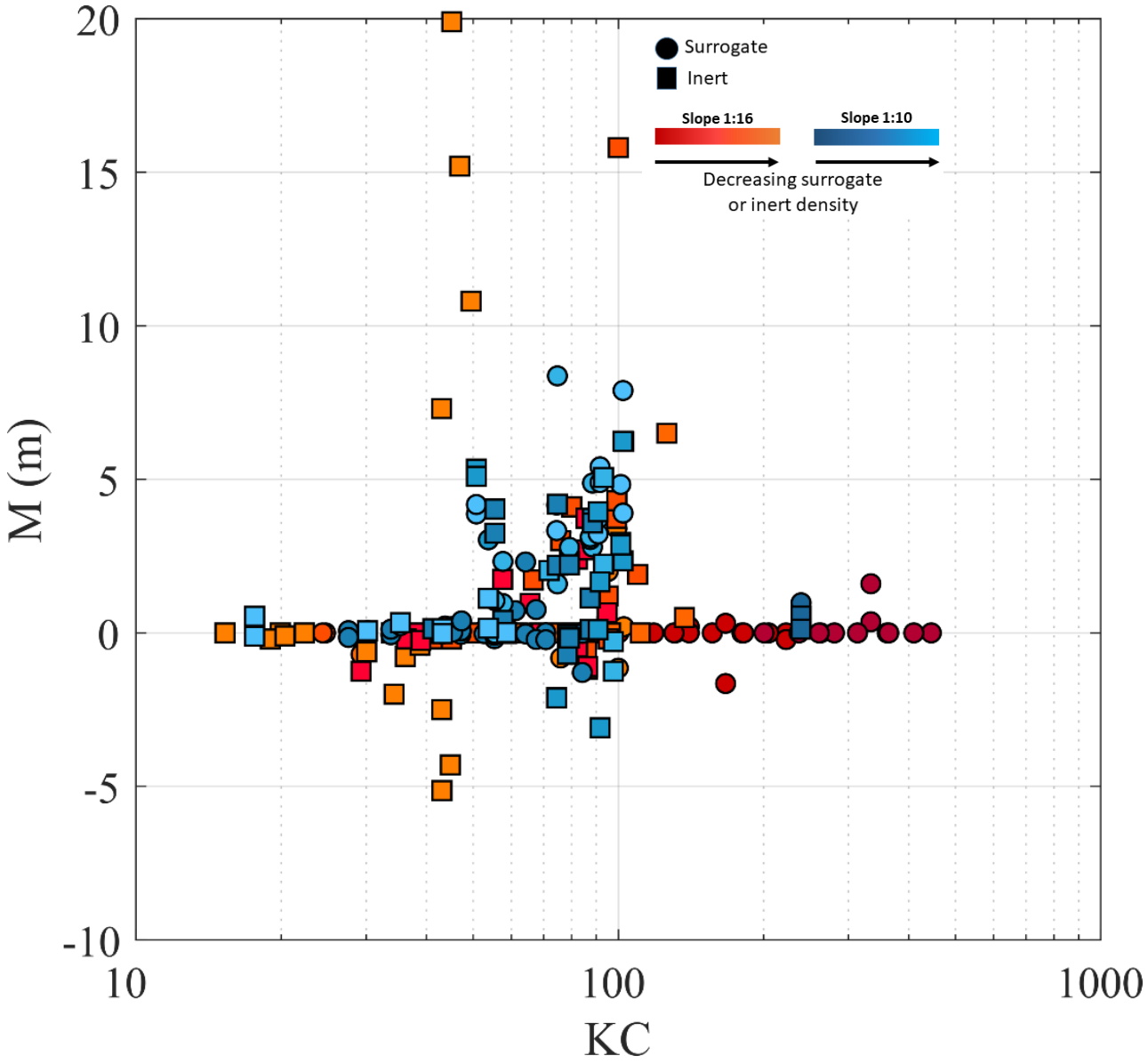

Figure 23. Cross-shore swash-zone surrogate and inert munitions migration as a function of object density, foreshore slope and Keulegan-Carpenter number. Density scale varies from roughly 3300 kg/m^3 to 8000 kg/m^3.

The relative burial depth does show some dependence with KC number (Figure 24) as has been found previously (Friedrichs et al., 2016). The dependence is not strong considering both parameters are on a log-log scale, but the data do cluster within previously determined relationships (Friedrichs et al., 2016) found for cylinders (Figure 24; black dashed line) and frustra (Figure 24; red dashed line). B/D shows a consistent trend with KC and object density. That is, the most dense objects generally have a larger relative burial depth with increasing KC number independent of beach slope.

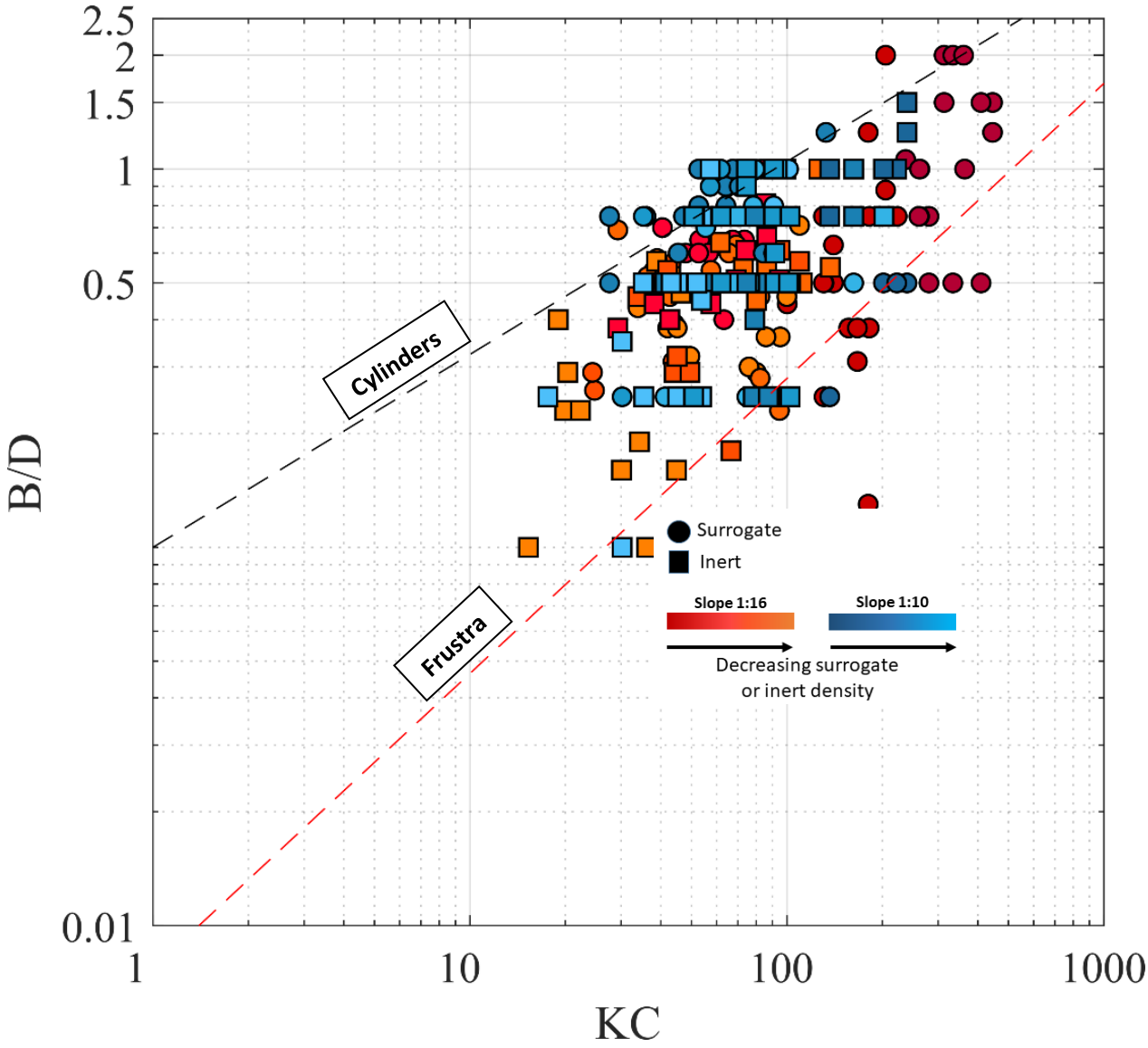

Figure 24. Relative burial depth of swash-zone surrogate and inert munitions as a function of object density, foreshore slope and Keulegan-Carpenter number. Density scale varies from roughly 3300 kg/m^3 to 8000 kg/m^3.

3.5 Surf zone surrogate and inert migration and burial

Surf zone surrogate and inert cross-shore position (Figure 25) and relative burial (Figure 26) are presented as a function of run number for the SUXOII study. Data are shown with corresponding maximum θ. Yellow symbols indicate the object was reset prior to the run commencing. There are no overarching trends in migration distance as a function of the forcing conditions. In fact, we find that the surrogate and inert munitions in the breaker zone migrated little. The largest migration distance was roughly 3 m onshore for a surrogate 81 mm mortar. The lack of migration can result from a variety of causes: breaker zone munitions may only migrate under extreme forcing; the underlying morphology may play a significant role in altering migration; the object density causes them to bury under local scour; or they were in deep enough water such that the forcing conditions were not great enough to cause migration.

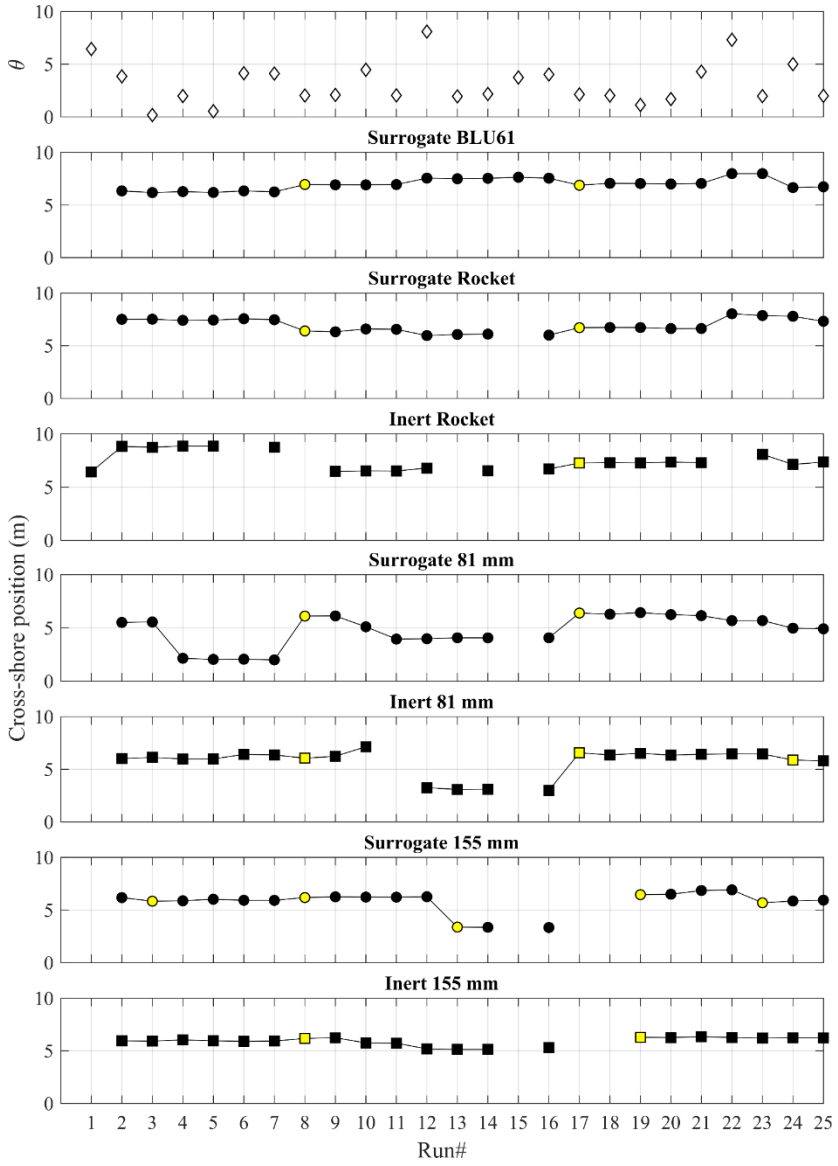

Figure 25. Cross-shore position of surrogate and inert munitions as a function of run number for the SUXOII study.

Surf zone surrogate and inert objects tended to self bury rather than migrate as identified by the estimated *B/D* ratio (Figure 26). Relative burial was on the order of 1 for the items deployed. Rockets and 81 mm mortars tended to bury the most but not enough objects were deployed to quantify this statistically (it is impractical to deploy enough of each of these munitions to determine this with statistical significance). Relative burial depth did not appear to be heavily influenced by forcing conditions suggesting prior attitude on the sea floor must also play a role in subsequent burial.

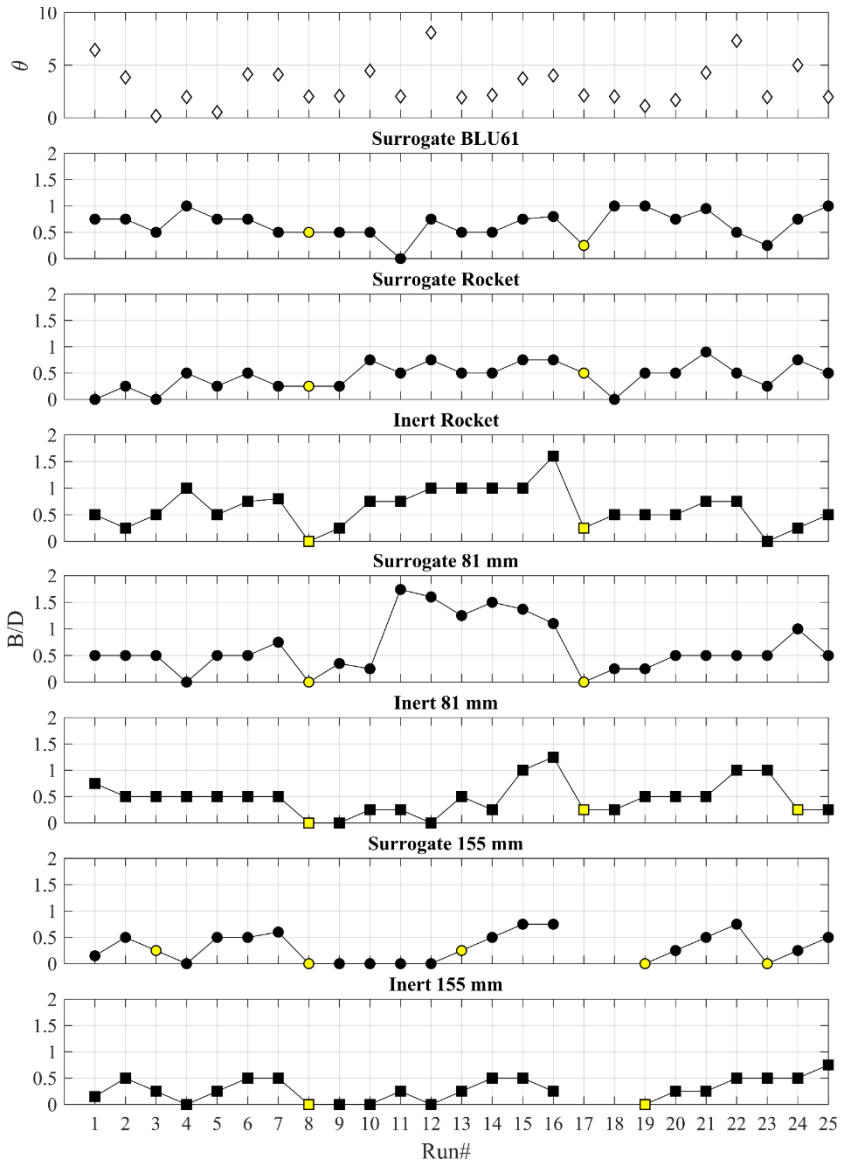

Figure 26. Relative burial of surrogate and inert munitions as a function of run number for the SUXOII study.

3.6 Example calculation of forces on surrogates in the swash zone

An object (Figure 27), proud or partially buried, immersed in a fluid experiences forces that can lead to migration (and burial).

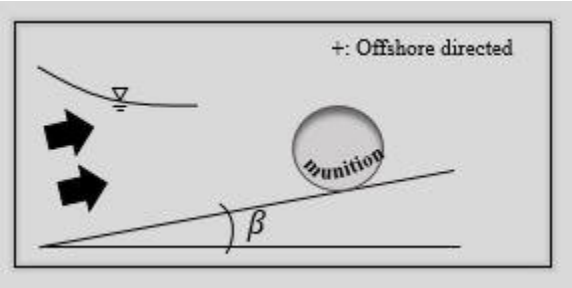

Figure 27. Schematic of munition on the beach face under hydrodynamic forcing.

We focus on the migration aspect using a prior formulation (Luccio et al., 1998) developed for cobbles on the beach face that relates the object acceleration (F_{am}) to fluid acceleration (F_{aflow}), drag (F_d) and lift (F_l) forces, reduced gravity ($Wsin\beta$) and bed friction (F_f) as

$$F_{am} = F_{aflow} + F_d + F_l - Wsin\beta - F_f. \quad (4)$$

Each term must be estimated from available data and many contain unknown or additional coefficients that must also be estimated (Table 6). Coefficient values can be mined from the literature but many are order 1 and for the initial analysis we use the value of 1 as a first estimate. There is an additional force identified in Table 6 associated with initial impact of the uprush. The term is referred to as the surge force and borrows from tsunami impact studies on infrastructure. The effect (force from) of this term may already exist in the simple formulation (eq. 4) but we choose to also investigate the importance of the initial impact. The surge force is applied only for ~0.25 s because it is associated with the initial swash impact.

Three examples of force calculations on a surrogate on the beach face are shown in Figures 28-30. The three figures have the same format. Water depth (top Panel) reaches roughly 0.3 m at its maximum as recorded by the frame PT and that in the surrogate (when available). Fluids velocities (Panel 2) reach nearly 2 m/s in magnitude and require the linear fit (described previously) to deal with signal discontinuity. The 81 mm mortar surrogate had a net onshore migration of approximately 0.05 m, but experienced both onshore and offshore motion (Figure 28, third Panel). Both rockets (SUDRKT2, Figure 29; SUDRKT1, Figure 30) had a net offshore migration of over 1 m with little onshore motion. The force balance is dominated by the drag (fluid on object) and the friction at the bed resisting motion (Panel 4). The sign on the friction term acts opposite to the surrogate motion. Onshore directed drag exceeds 50 N, while the friction magnitude is less than 50 N and constrained mostly by the cosine of the beach slope. The other terms in the balance are quite negligible, specifically the fluid and surrogate acceleration. Surprisingly, from an intuition standpoint, the reduced gravity term is also negligible. We would have expected the steep slope to cause this term to be more important to force balance. However, even for steep beaches the sine of the beach slope is on the order of 0.1. Altering the coefficients

for the terms in the force balance could change the relative importance of a given term. We will investigate coefficient variability in subsequent analysis. The dynamic surge force, that cannot be considered separately in the force balance, represents a momentum flux on one side of the surrogate and has a magnitude that exceeds the other forces. It must certainly be important for the onshore portion of the surrogate motion.

*Table 6. Quantification of the terms in the force balance of an object on the beach face.**

Force	Parametrization	Measurements	Coefficients
Munition acceleration	$(\rho_m + \rho C_m) V_m \frac{dU}{dt}$	$\frac{dU}{dt}$	C_m
Fluid acceleration	$(1 + C_m) \rho V_m \frac{du}{dt}$	u	C_m
Drag	$\frac{C_d}{2} \rho A_d \rho u \lvert u \rvert$	u	C_d
Lift	$\frac{C_l}{2} \rho A_l \rho u \lvert u \rvert$	u	C_l
Reduced gravity	$(\rho_m - \rho) V_{sub} g sin\beta$	β	
Friction	$C_f (\rho_m - \rho) V_m g cos\beta$		C_f
Surge	$\frac{1}{2} \rho g h^2 L + \rho u \lvert u \rvert h L$	h, u	

***** ρ_m is the munition density, ρ is the fluid density, L is the munition length, V_{sub} is the submerged munition volume, V_m is the munition volume, A_d is the projected munition area for drag, A_l is the projected munition area for lift, C_m is the added mass coefficient, C_d is the drag coefficient, C_l is the lift coefficient, C_f is the friction coefficient, U is the munition velocity, u is the fluid velocity, h is the water depth and β is the slope angle.

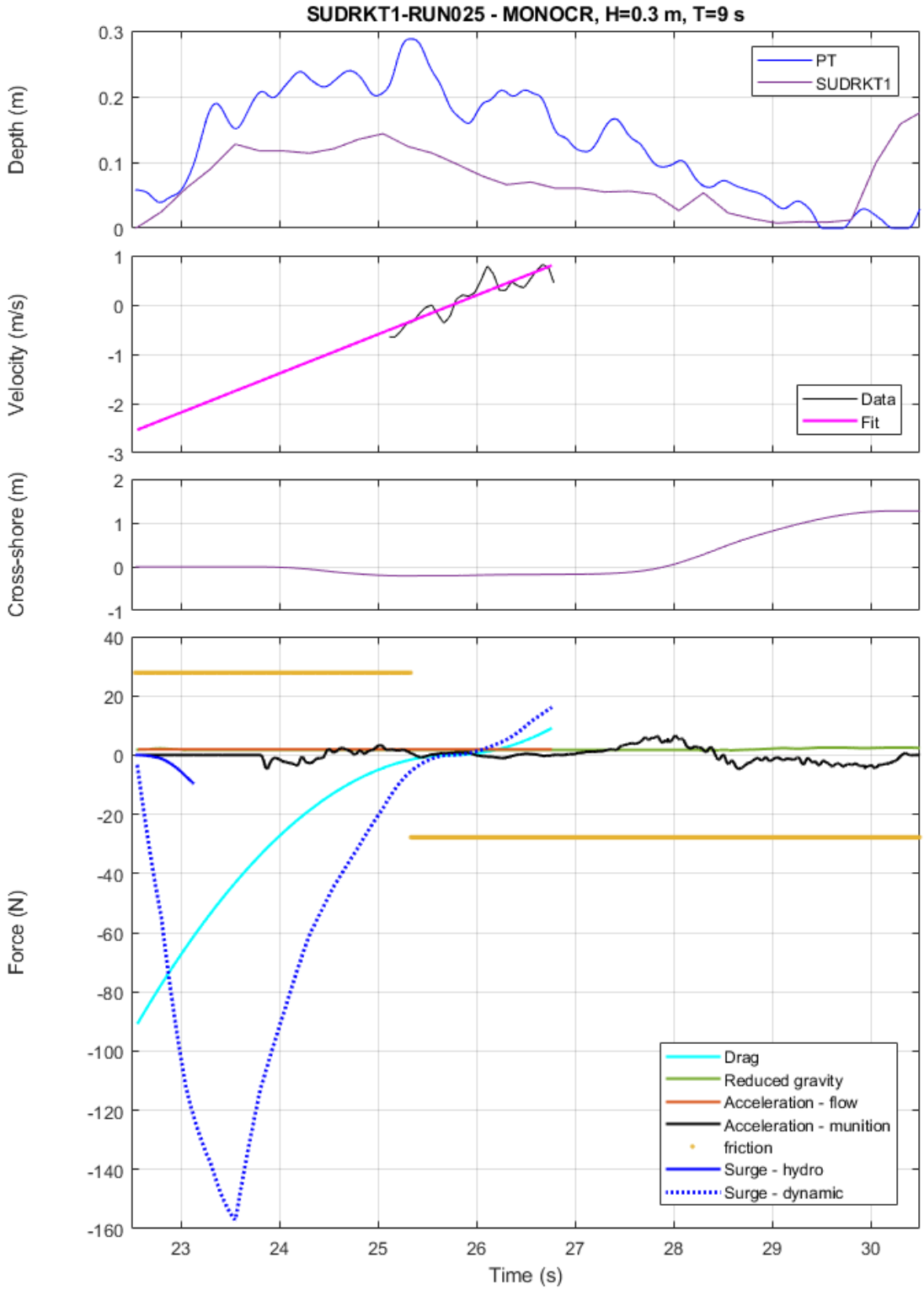

Figure 28. Example force calculation for an 81 mm mortar surrogate. Water depth (top Panel), velocity (2nd Panel), surrogate migration (3rd Panel), forces from equation (4) (4th Panel).

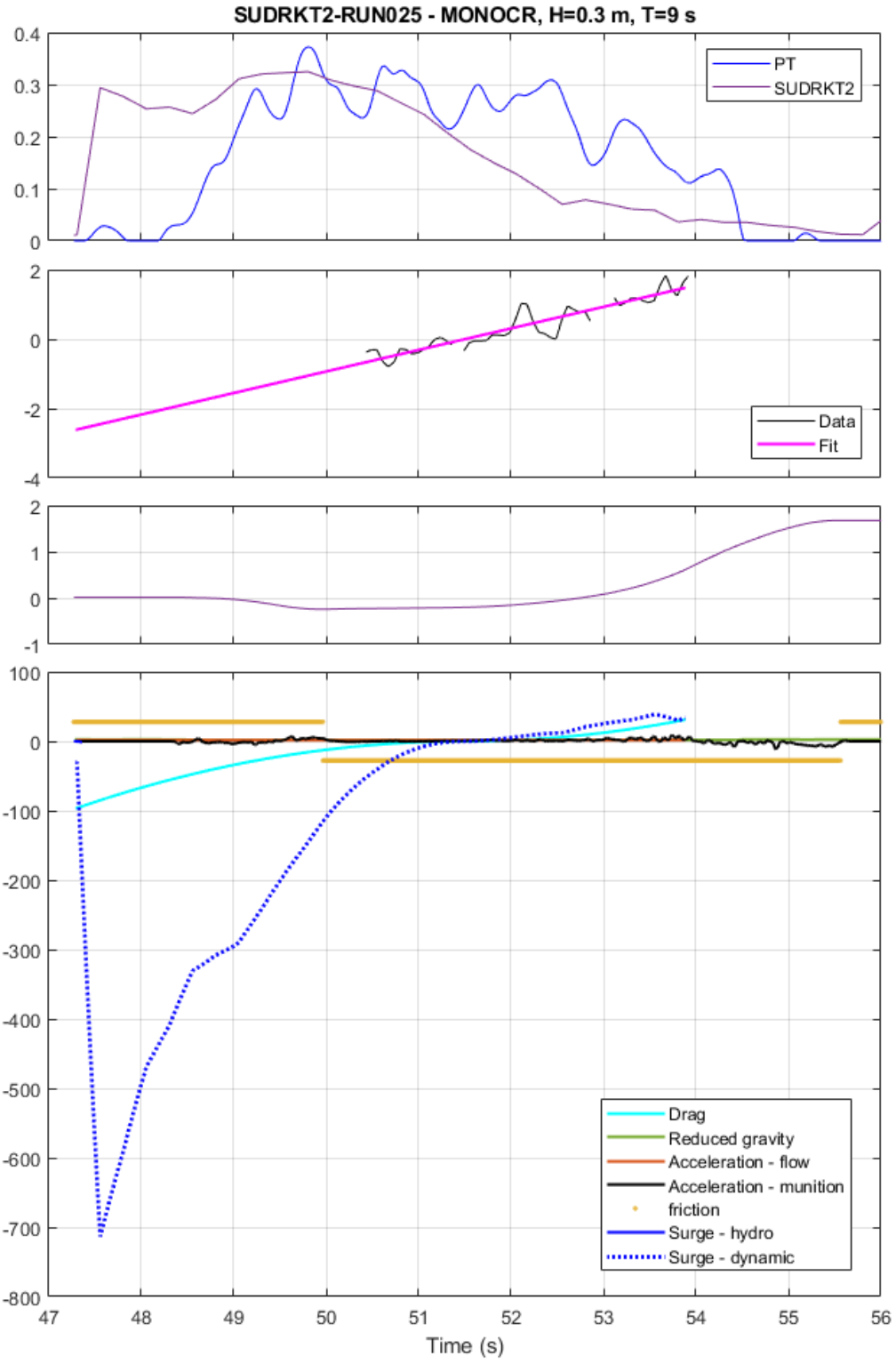

Figure 29. Example force calculation for a Hydra Rocket (RKT2) surrogate. Water depth (top Panel), velocity (2nd Panel), surrogate migration (3rd Panel), forces from equation (4) (4th Panel).

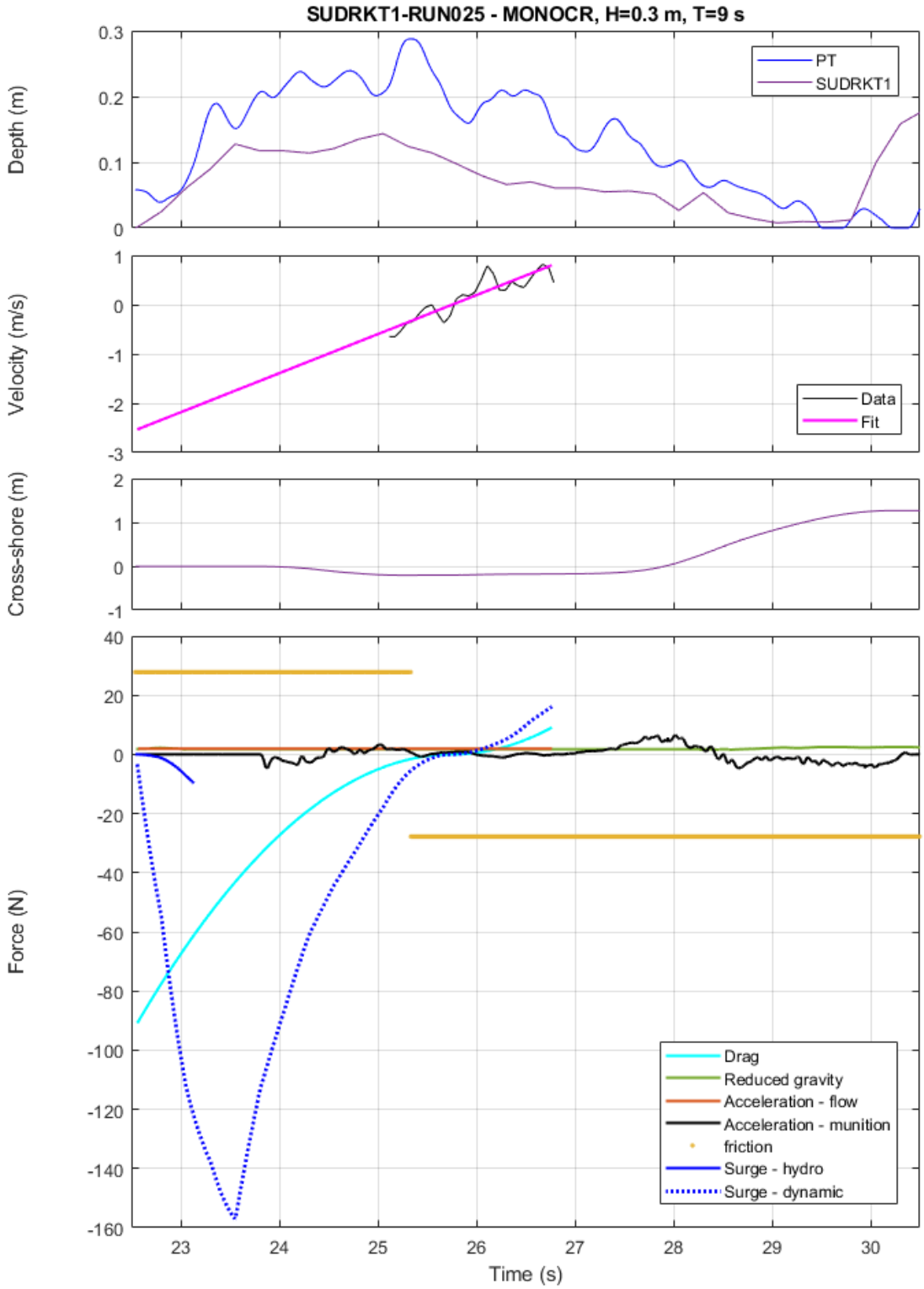

Figure 30. Example force calculation for a Hydra Rocket (RKT1) surrogate. Water depth (top Panel), velocity (2nd Panel), surrogate migration (3rd Panel), forces from equation (4) (4th Panel).

3.7 Summary and Ongoing Analyses

Surrogate and inert munitions migration and burial were quantified/estimated using GPS, image analysis and inertial motion units during two large-scale laboratory studies (SUXOI and SUXOII). We find that surrogate and inert munitions on the beach face are highly mobile unlike those observed farther offshore in the breaker or shoaling zones. Overriding factors for mobility are the high fluid velocities and shear stresses and the steep foreshore slopes where the downslope component of gravity is important. It cannot be overlooked, however, that some munitions migrated landward even on the steep slopes in the studies. There did not appear to be overarching relationships between either the Shields number or the Keulegan-Carpenter number in terms of migration. More energetic forcing sometimes caused larger migration distance but not always. The most dense objects had larger relative burial depths than less dense objects as a function of either Shields number or the Keulegan-Carpenter number. The relative burial depth data for cylinders and frustra were bounded by the relationships relative to the Keulegan-Carpenter number found previously (Friedrichs et al., 2016). At present, the object diameter is used in the denominator of KC. Future efforts may require using the munition orientation relative to the flow to modify this value. If the longitudinal axis is parallel to incoming waves (perpendicular to the cross-shore velocity), then the object length or some parameterization of it may be more relevant for the KC calculation.

Observations show that surrogate and inert munitions can sometimes behave similarly and other times not. Even two surrogates placed side by side under the same forcing conditions may behave differently. That is, some observations showed some munitions migrating offshore while others remained fixed in place or moved onshore. The variability observed means that many more realizations are needed to tease out and quantify the variability. We believe the differences may be due to small morphologic variability not captured by our data collection methods (perhaps related to, for example, a pebble located a short distance from the munition, or other bathymetric anomaly). There may be other reasons for the observed differences. Turbulence variability from one alongshore location to another could occur. The offshore forcing conditions are considered the same, but offshore bathymetry can alter local shoaling and refraction that may cause local alongshore variations on the beach face. Any small variations, that could be important, are difficult to quantify.

Terabytes of data (much of it video) were collected during both studies. Data quality control and cleaning is essentially complete and efforts are now (and have been) largely focused on data analysis with the major efforts related to extracting migration from inertial motion unit data and video sequences and trying to relate that migration back to the forcing, including from force balance arguments. Several force balance examples were shown here and the analysis will continue with each instant we can identify in the video sequences when a surrogate or inert munition is initially impacted by a swash front. The data generated from these studies is soon to be used by other project partners. A meeting has been set up with Sarah Rennie (April 2018) so we can transition our findings to use in the UnMES model.

Logistics and science planning are underway for the final field deployment as part of this project. The field effort is slated to occur at Wallops Island, VA (NASA facility) from mid-August to roughly mid-November, 2018. We choose a fall time frame in the hopes of capturing higher

energy conditions. Wallops Island is an ideal location because it is federal property allowing us to deploy surrogates without significant worry about loss and because of the logistical support NASA can provide. Prior efforts were only roughly 2 weeks in length which did not provide enough time to obtain long time series of munition migration. We will install a fence offshore (similar to SUXOII) to prohibit surrogate and inert munitions from leaving the study area. This feature was not described in the original proposal but we believe it is necessary given the inability to control offshore migration distances of munitions. Tethering munitions is not deemed appropriate as that alters mobility characteristics. The alterations were observed during the previous WIMMX study.

Products: We have presented our research at seven conferences and are slated to present the findings at the European Geophysical Union Conference in April. A paper on the smart munitions is in revision with IEEE Journal of Oceanic Engineering with an anticipated publication date of summer 2018. We will begin working on the next paper related to observations of munitions migration under large-scale forcing.

The project is at a Go/No-Go decision point for the final field deployment to occur during the summer/fall of 2018. The Go/No-Go criterion as mentioned in the project brief to the Scientific Advisory Board (SAB; October 21, 2014) and in the final proposal is based on adequate progress from the laboratory studies and data analysis in consultation with SERDP program managers. We recommend project continuation based on the significant progress thus far. We will conduct the final field effort following consultation with SERDP program managers. We will (already have) invited other SERDP researchers to participate in the field effort to enhance the study.

References

Friedrichs, C.T., Rennie, S.E., Brandt, A., 2016. Self-burial of objects on sandy beds by scour: A synthesis of observations, in: Scour and Erosion. CRC Press, pp. 179–189.

Holland, K.T., Holman, R.A., Lippmann, T.C., Stanley, J., Plant, N., 1997. Practical use of video imagery in nearshore oceanographic field studies. IEEE Journal of Oceanic Engineering 22, 81–92.

Luccio, P.A., Voropayev, S.I., Fernando, H.J.S., Boyer, D.L., Houston, W.N., 1998. The motion of cobbles in the swash zone on an impermeable slope. Coastal Engineering 33, 41–60.

Puleo, J.A., Holland, K.T., 2001. Estimating swash zone friction coefficients on a sandy beach. Coastal Engineering 43, 25–40.

Rennie, S.E., Brandt, A., Friedrichs, C.T., 2017. Initiation of motion and scour burial of objects underwater. Ocean Engineering 131, 282–294.